NPS-52MV8081A

UNITED STATES
NAVAL POSTGRADUATE SCHOOL

AN EXPERIMENTAL INVESTIGATION OF ASYNCHRONOUS

DEMODULATION OF A PHASE-REVERSAL-MODULATED CARRIER

by

Francis Albert Rudolph, Jr.

and

Glen A. Myers

August 1968

AN EXPERIMENTAL INVESTIGATION OF ASYNCHRONOUS DEMODULATION OF A PHASE-REVERSAL MODULATED CARRIER

by

Francis Albert Rudolph, Jr.
Commander, United States Navy

and

Glen A. Myers
Associate Professor of Electrical Engineering
Naval Postgraduate School
Monterey, California

August 1968

This task was supported by Naval
Ship Systems Command, Code 6050 in
Washington, D. C.

NAVAL POSTGRADUATE SCHOOL
Monterey, California

Rear Admiral R. W. McNitt, USN
Superintendent

R. F. Rinehart
Academic Dean

ABSTRACT:

This report considers an asynchronous (non-coherent) method of demodulating a carrier that is phase-reversal modulated by a two-level waveform. The comparatively simple demodulation technique treated relies on the conversion of a phase-modulated (PM) signal to an amplitude-modulated (AM) signal by appropriate filtering of the frequency components of the received phase-reversal modulated carrier. The resulting AM signal is then detected with a conventional envelope detector and the digital data is recovered with appropriate threshold and logic circuits.

The experimental asynchronous demodulation system requires approximately 12 db greater signal-to-noise power ratio for the same probability of error relative to the optimum performance of the coherent demodulation system. Thus with a signal-to-noise ratio of 18 db or greater, the asynchronous demodulation system has a measured probability of error of 10^{-3} or less; a signal-to-noise ratio of 23 db provides a measured probability of error of about 10^{-5}. Apart from simplicity, the asynchronous demodulation system has the advantage of not requiring prior knowledge of the transmitted signal's precise characteristics as is required in some coherent demodulation systems.

This task was supported by: Naval Ship Systems Command (Code 6050)

TABLE OF CONTENTS

LIST OF ILLUSTRATIONS

TABLE

LIST OF SYMBOLS

f	Frequency in Hertz
f_m	Modulation frequency in Hertz
f_o	Carrier frequency in Hertz
$r(t)$	Locally generated replica of the carrier
$s(t)$	Coherent demodulator output signal
t	Time in seconds
$v(t)$	Carrier signal (volts)
$v_f(t)$	Bandpass filter output voltage
$v_u(t)$	Highpass filter output voltage
A	Constant peak amplitude of the carrier
B	Bandwidth in Hertz
E	Energy per bit (in watt-seconds per bit)
$E(t)$	Modulating signal
N_o	Constant noise power spectral density
P_{avg}	Average signal power
P_e	Probability of error
T_d	Width of the pulse width discriminator window
T_m	Modulation period in seconds
V_d	Threshold voltage level
V_n	RMS value of noise
V_s	RMS value of v(t)
$V(f)$	Fourier transform (one-sided voltage spectrum) of v(t)
$V_f(f)$	Fourier transform (one-sided voltage spectrum) of $v_f(t)$
$V_u(f)$	Fourier transform (one-sided voltage spectrum) of $v_u(t)$
X_n	Noise envelope
X_s	Envelope of $v_f(t)$
X_{sn}	Envelope of the quantity $v_f(t)$ plus added noise

$\hat{X}_s$	Envelope peak-to-valley voltage difference of $v_f(t)$
δ	Dirac delta function
$\Theta(t)$	Carrier phase modulation term
$\omega = 2\pi f$	Radian frequency
$\omega_m = 2\pi f_m$	Radian modulation frequency
$\omega_o = 2\pi f_o$	Radian carrier frequency

ACKNOWLEDGEMENTS

The authors are pleased to acknowledge the support of Naval Ship Systems Command (Code 6050) in this study. We wish to thank Mrs. Nancy Lawrence for her contribution in the typing and preparation of this report.

Chapter 1

INTRODUCTION

In the past decade the rise to prominence of digital data transmission systems has been the result of a number of scientific requirements and developments which include telemetry and data processing by digital computers. Today such computers are linked by digital data networks; data, telemetry and control signals are commonly transmitted over digital data links; some communication satellites use digital transmission systems; the commercial telephone system uses digital signals to transmit voice and television signals over land lines as well as radio-frequency links [Ref. 1]. Digital data may assume a variety of forms with the binary or two-symbol signal being the most common.

Radio transmission of binary signals requires a radio-frequency carrier modulated by the discrete waveform representing the information to be transmitted. Various forms of carrier modulation are possible such as on-off keying, frequency-shift keying, phase-shift keying, etc. Of the various types of modulation tabulated by Bennett and Davey [Ref. 2, pp. 225-39], coherent binary phase modulation or phase reversal modulation (PRM) ranks highest in almost all categories of performance. For example, PRM provides the lowest probability of error for a given signal-to-noise power ratio [Ref. 3].

Bennett and Davey [Ref. 2, p. 238, Table 11-2] also note that the coherent types of binary phase-modulation systems are generally more complex to instrument. This is because coherent demodulation requires the mixing (multiplication) of the received signal with a replica of the transmitted signal. This replica is produced in the receiver and requires prior knowledge by the receiver of the transmitted waveform characteristics such as carrier frequency or data rate. This knowledge

is then applied in the design of the demodulator. This required relation between the demodulator characteristics and the transmitted waveform not only introduces complexity but also prevents use of a given demodulator with other similar systems.

This study investigates an asynchronous (non-coherent) method of demodulating a PRM carrier. This comparatively simple demodulation technique relies on the conversion of a phase-modulated (PM) signal to an amplitude-modulated (AM) signal by appropriate filtering of the frequency components of the received PRM carrier. The resulting AM signal is then detected with a conventional envelope detector and the digital data is recovered with appropriate threshold and logic circuits.

A. PRM Systems

Fig. 1 is a block diagram of a basic PRM transmitting system and shows typical waveforms. The phase-reversal modulator in Fig. 1 is usually a balanced mixer as explained in Chapter 4. Depending on the particular coherent demodulation technique, it may be necessary to maintain close tolerance on the carrier frequency f_o, the carrier phase or the data rate at the transmitter.

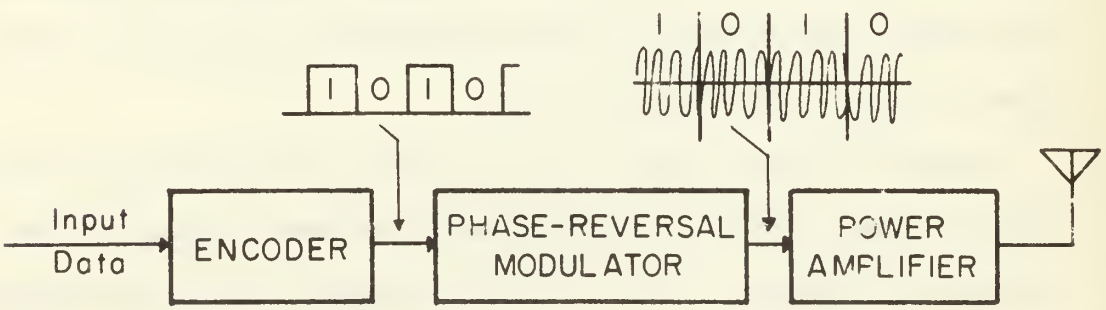

FIG. 1. BLOCK DIAGRAM OF A TRANSMITTING SYSTEM USING PHASE-REVERSAL MODULATION.

Demodulation of a phase-reversal modulated (PRM) signal by a coherent or differentially coherent process requires some knowledge of the transmitted signal's characteristics. Fig. 2 is a block diagram of a typical coherent demodulation system. The reference carrier is

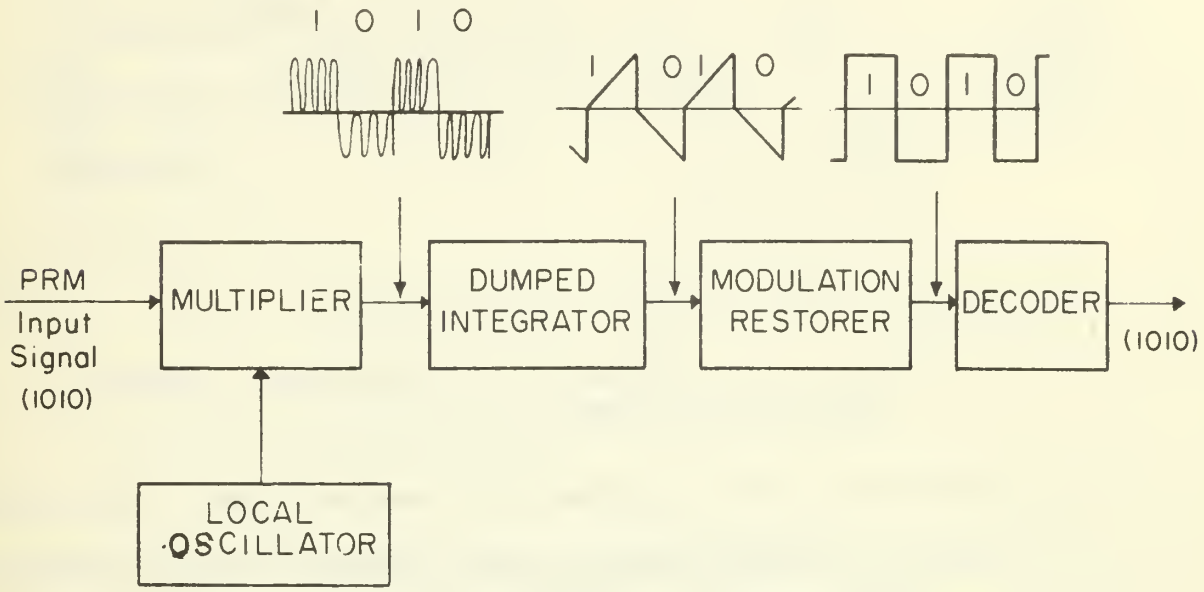

FIG. 2. BLOCK DIAGRAM OF A COHERENT DEMODULATION SYSTEM.

often generated by a highly stable local oscillator or by a phase-locked loop. Postdetection processing of the signal may take many forms. The differentially coherent demodulation system shown in Fig. 3 uses a delay line to permit correlation of the waveform in the present pulse interval with that in the preceding interval to establish the crosscorrelation product as either positive (no change of phase) or negative (change of phase). The differentially coherent demodulation system requires knowledge of the data rate by the receiver. The systems of Figs. 2 and 3 have nearly equal performance [Ref. 3].

In an asynchronous demodulation system, it is assumed that the phase and frequency of the received carrier are not precisely known

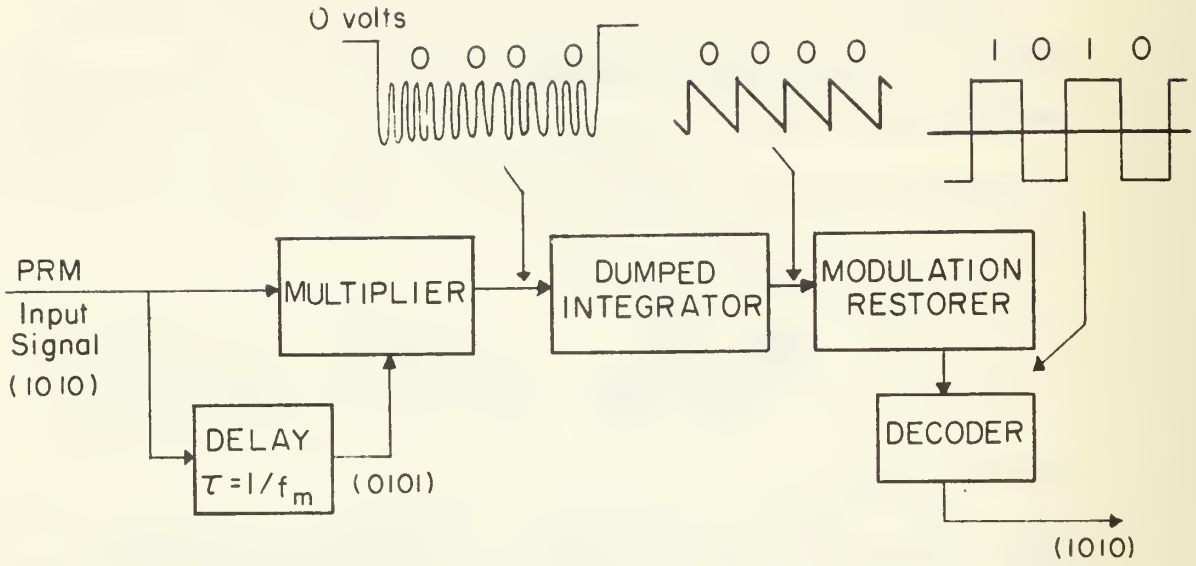

FIG. 3. BLOCK DIAGRAM OF A DIFFERENTIALLY COHERENT DEMODULATION SYSTEM.

and that the data rate is neither well known nor fixed. It is apparent that there is a penalty associated with this lack of prior knowledge of the signal parameters. It is shown experimentally in this report that this penalty is an approximately 12 db greater signal-to-noise power ratio required by a particular asynchronous demodulation system as compared to the coherent systems for the same probability of error of the recovered digital data. This degraded performance is offset in part by the simplicity of the design and the operation of the asynchronous demodulation system. Fig. 4 is a block diagram of the asynchronous demodulation system considered in this report. The filter used in the experiment is a mechanical bandpass filter which serves as the PM-to-AM transducer. The operation of this system is explained in detail in Chapter 4.

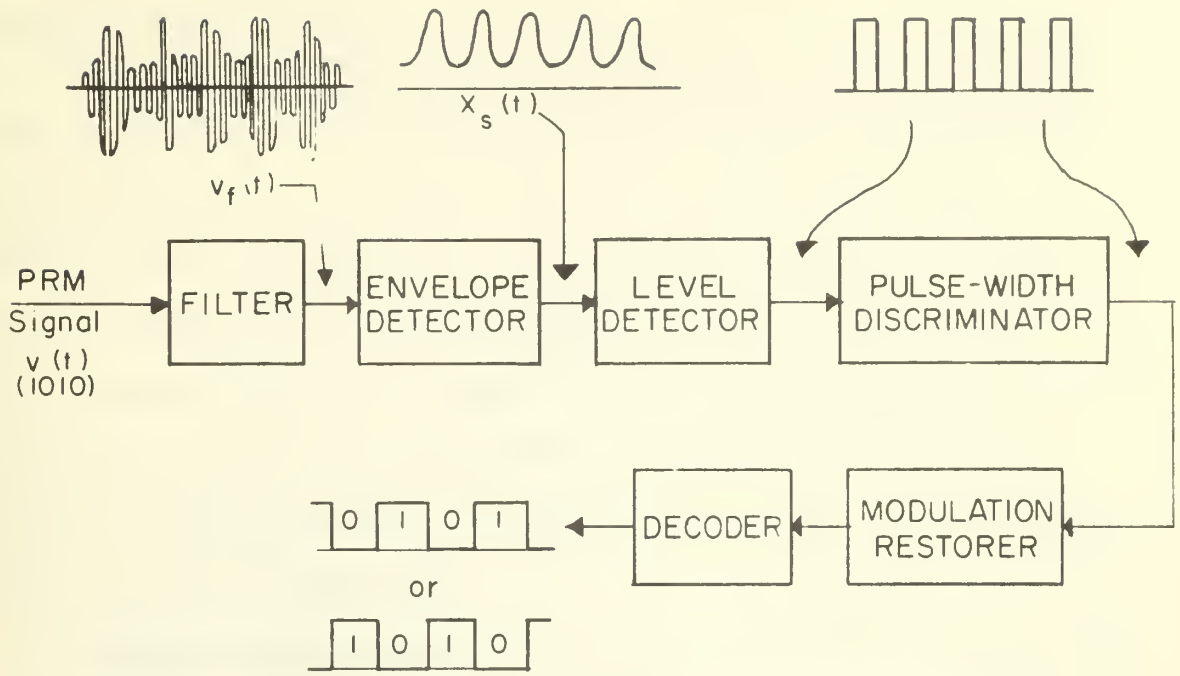

FIG. 4. BLOCK DIAGRAM OF AN ASYNCHRONOUS SYSTEM TO DEMODULATE A PHASE-REVERSAL MODULATED CARRIER.

B. Plan of the Report

In Chapter 2 the theoretical performance and the experimental results obtained using a coherent demodulation system are compared. The experimental results, which indicate the probability of error vs signal-to-noise power ratio performance of the asynchronous demodulation system, are presented.

An analysis of coherent demodulation systems is presented in Chapter 3. The results of a computer-aided analysis of the amplitude-modulated carrier envelope of the filter output of the asynchronous demodulation system is also presented in Chapter 3.

Chapter 4 details the experimental procedure and describes the circuitry and operation of the major elements of the experimental PRM

modulator, the coherent demodulator and the asynchronous demodulator.

Conclusions and recommendations are presented in Chapter 5. Appendices A and B present details supporting the material in the body of the report. A list of references is provided.

Chapter 2

RESULTS

This chapter presents the experimental and some analytical results pertaining to the coherent and to the asynchronous demodulation systems considered. Using these results, a comparison of these two types of systems is possible. With a coherent demodulation system of the type shown in Fig. 2 a probability of error of 10^{-3} at a SNR of 7.3 db is obtained. This study shows that with an asynchronous demodulation system like that of Fig. 4 a probability of error of 10^{-3} can be exprected at a SNR of 18 db; with a SNR of about 22 db, a probability of error of 10^{-5} can be expected.

A. Coherent Detection System

Lawton [Ref. 4], Cahn [Ref. 5] and others have calculated the theoretical probability of error P_e as a function of the signal-to-noise power ratio (SNR), or alternatively as a function of the ratio of energy per bit to noise power per Hertz of bandwidth, for various types of modulation. Additionally, these authors present experimental results indicating that in practice the theoretical performance curves are shifted to the right (higher SNR for the same P_e) by 0.5 to 1.0 db. Fig. 5 presents Cahn's results showing the theoretical coherent demodulation system's performance and a number of experimentally determined performance points. Fig. 5 also shows the experimental results obtained from this study. The system used to obtain the data of Fig. 5 is considered in Chapter 4 of this report.

In practical applications the transmitted signal would normally be band limited to conserve the frequency spectrum. The analysis in Chapter 3 of a PRM carrier modulated by a square wave shows that when the transmitted signal consists of only four side frequencies (the

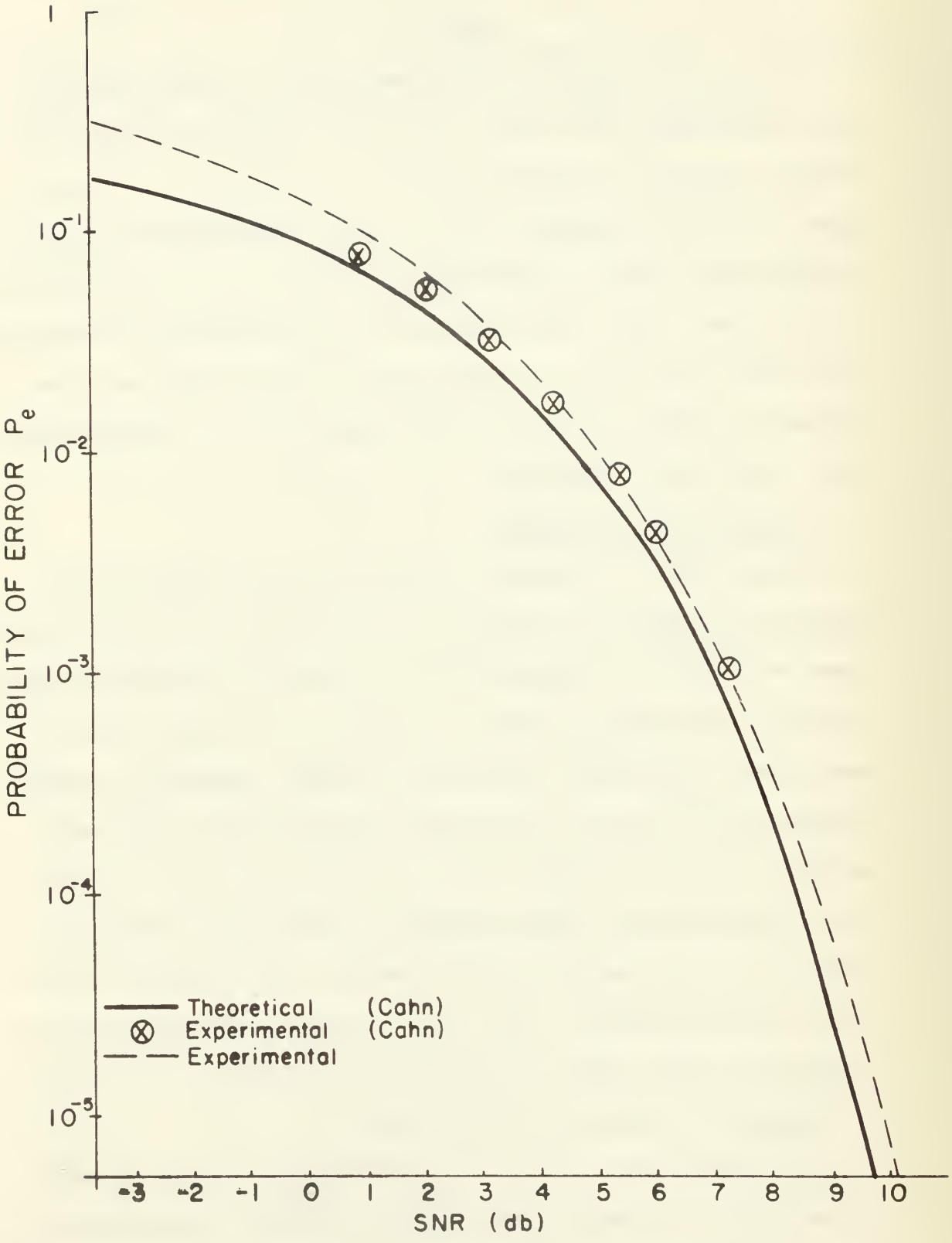

FIG. 5. A PLOT OF THE THEORETICAL AND EXPERIMENTAL PERFORMANCE OF A COHERENT DEMODULATOR.

first two non-zero upper and first two non-zero lower spectral components) a degradation in performance of only about 0.5 db relative to the wideband (unfiltered) case results. The coherent demodulation system would normally be equipped with a predetection bandpass filter to limit total noise power and reject undesirable harmonically related spurious frequency components. When the data rate is lower than the maximum allowed by the bandpass predetection filter an additional degradation in performance of up to 1.6 db can result. For example in a coherent demodulation system with a 50 kHz predetection bandpass filter, the coherent demodulator performance curve is located about 1.5 db to the right of the optimum performance curve shown in Fig. 5 when the carrier is PRM by a square wave which switches at a 10.6 kHz rate.

B. Asynchronous Demodulation System

Four basic factors affect the performance of the asynchronous demodulation system. These factors are (1) received signal-to-noise ratio (SNR), (2) the number and weighting of the spectral components at the output of the bandpass filter, (3) the threshold level V_d of the level detector and (4) the width T_d of the time window of the postdetection pulse-width discriminator. (See Fig. 6 for a definition of V_d, T_d and other parameters.) All but the SNR are controllable in the asynchronous system which is considered in detail in Chapter 4 of this report.

The effect, as determined experimentally, of using a pulse width discriminator (PWD) in the postdetection processing of the detected signal is shown in Fig. 7. An improvement in SNR of about 1.0 db at a P_e of 10^{-3} and about 3.0 db at a P_e of 10^{-5} is realized by using the

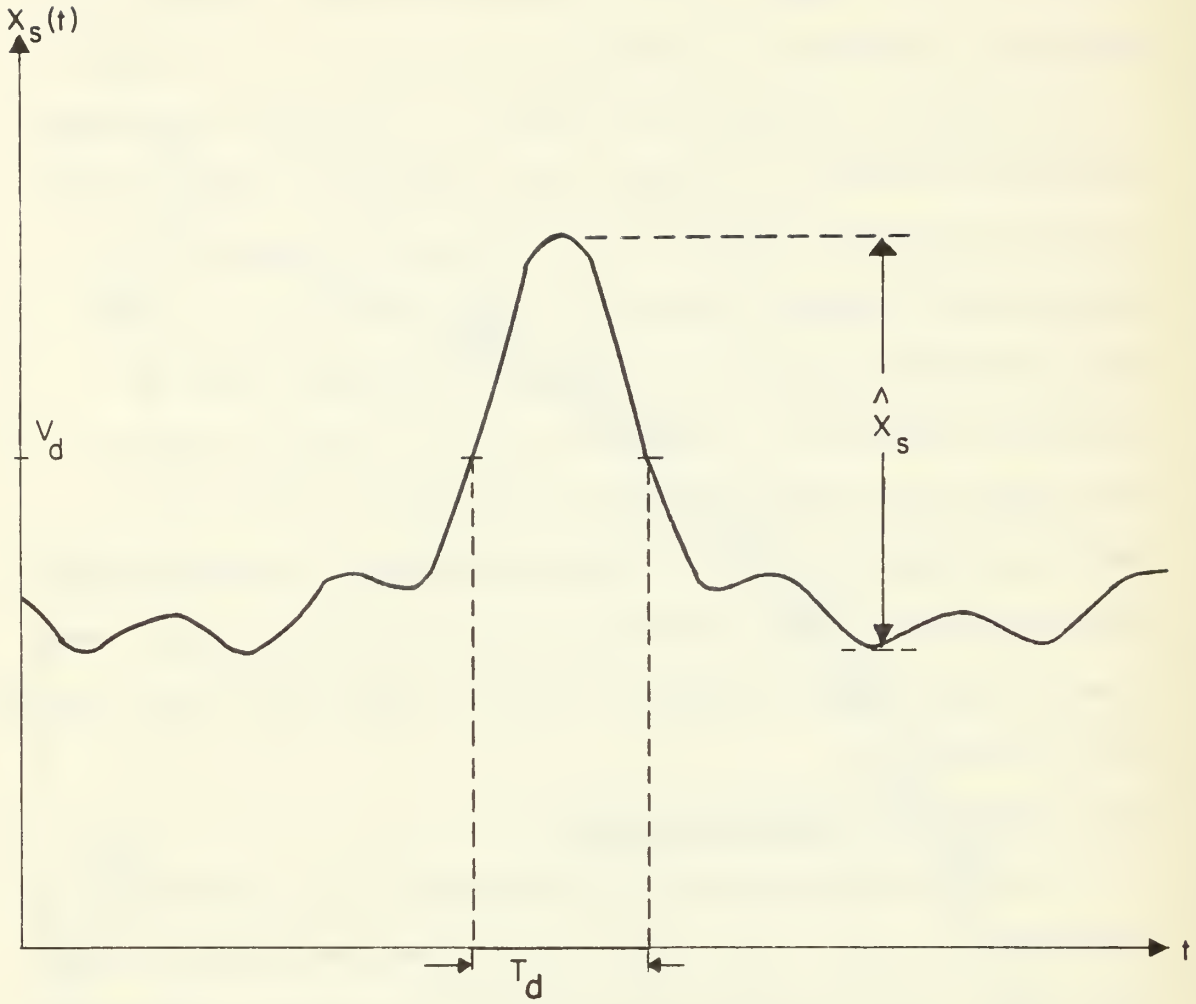

FIG. 6. A TYPICAL ENVELOPE $X_s(t)$ OF THE PM-TO-AM CONVERTER SHOWING SYSTEM PARAMETERS V_d, T_d AND $\hat{X}_s$.

PWD. It was found in the experiment that there is a range of settings of T_d over which no detectable difference in system performance is noted. In each of the experiments T_d was adjusted to the value which produced the best measured performance at a SNR of 20 db.

The curves of Fig. 8 show the effect on the asynchronous demodulator performance when the level detector threshold voltage V_d is

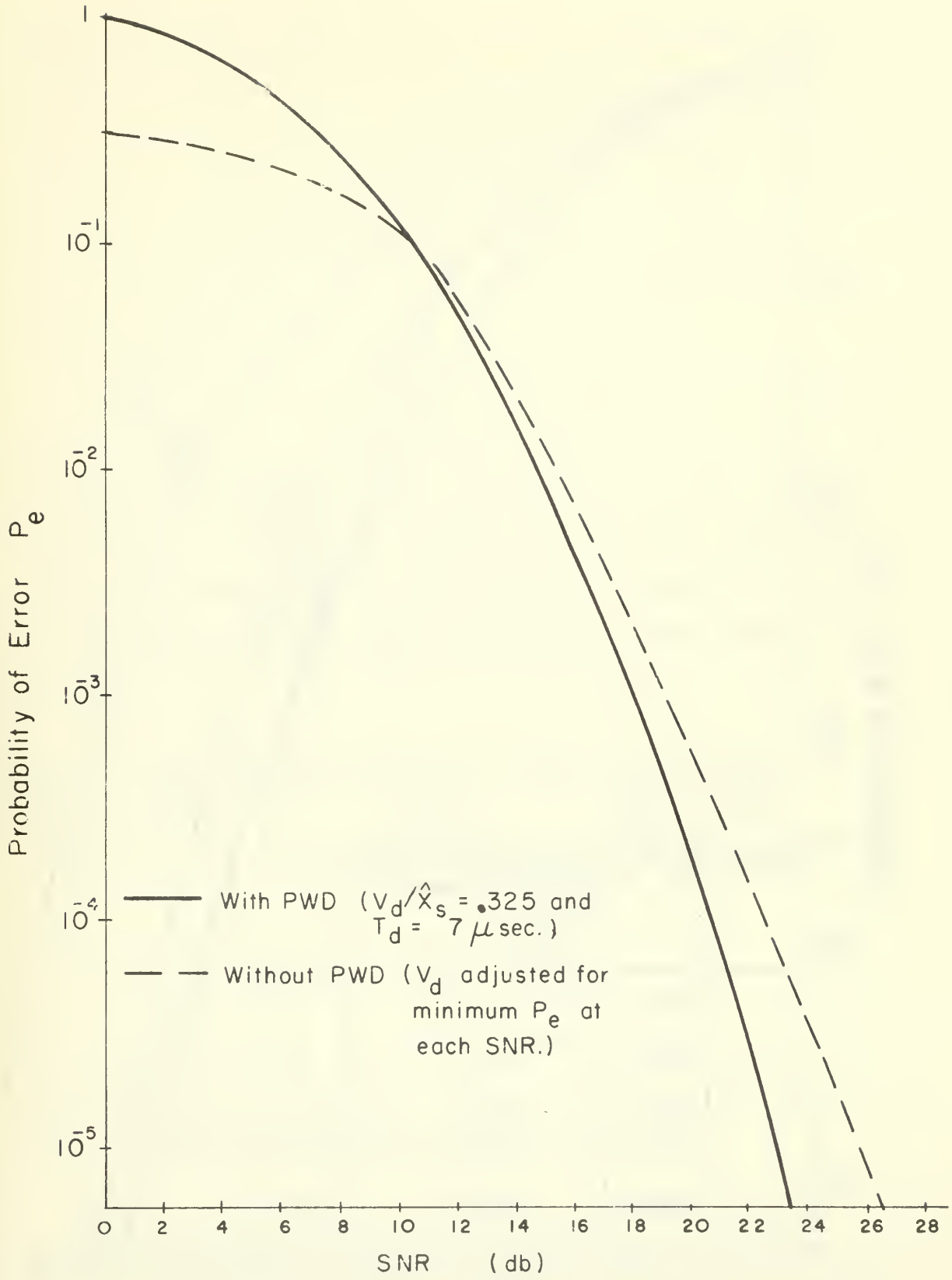

FIG. 7. A PLOT OF THE PERFORMANCE OF AN ASYNCHRONOUS DEMODULATION SYSTEM WITH AND WITHOUT A PULSE-WIDTH DISCRIMINATOR (PWD). The carrier is phase-reversal modulated by a square wave. Four spectral components of the filtered carrier are retained.

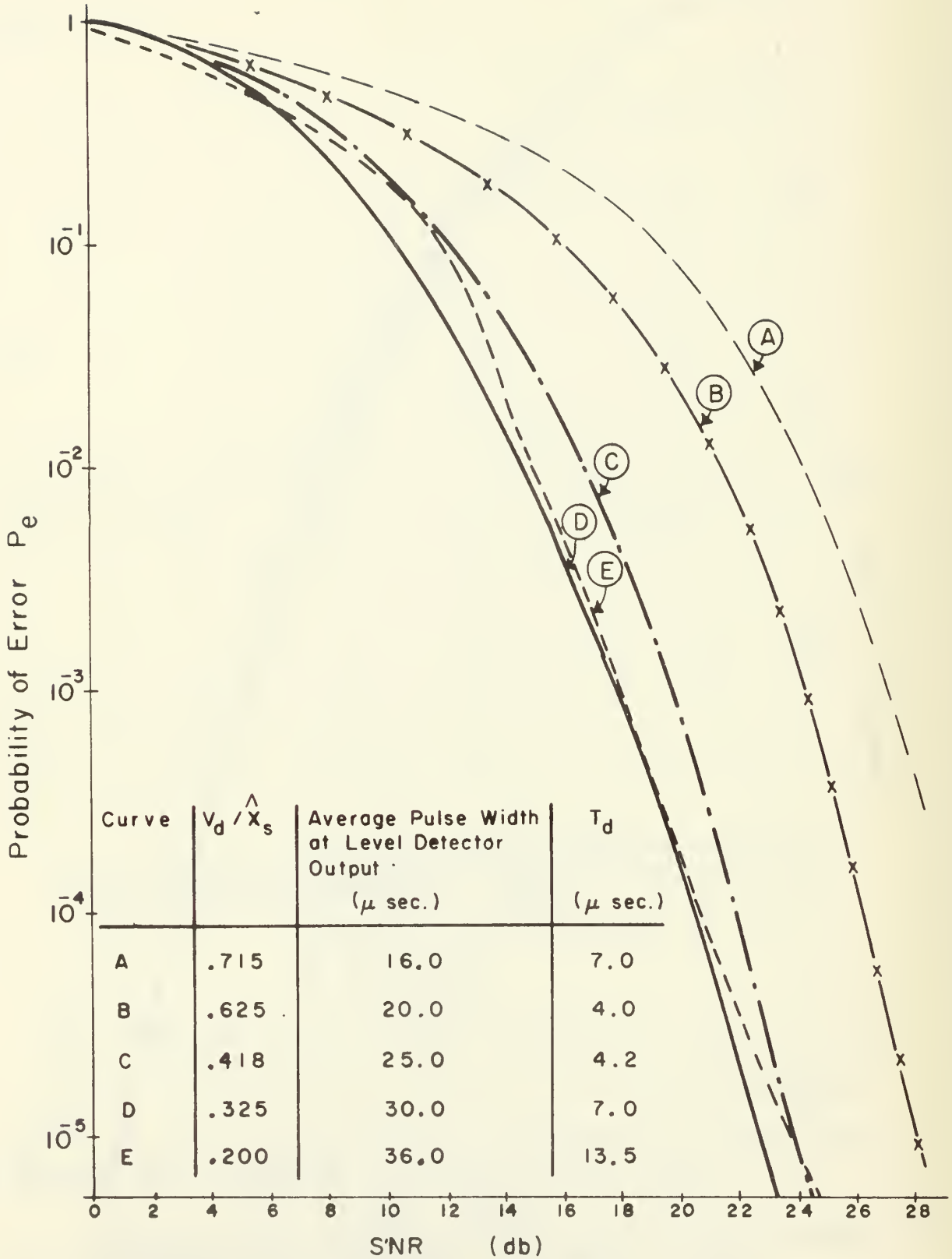

Curve	$V_d / \hat{X}_s$	Average Pulse Width at Level Detector Output (μ sec.)	T_d (μ sec.)
A	.715	16.0	7.0
B	.625	20.0	4.0
C	.418	25.0	4.2
D	.325	30.0	7.0
E	.200	36.0	13.5

FIG. 8. A PLOT OF THE PERFORMANCE OF AN ASYNCHRONOUS DEMODULATION SYSTEM FOR DIFFERENT VALUES OF THRESHOLD LEVEL V_d. The carrier is phase-reversal modulated by a square wave. Four spectral components of the filtered carrier are retained.

varied. The filter output spectrum consists of four upper side frequencies of the square-wave modulated PRM carrier. In each case, a value of threshold voltage V_d relative to the peak-to-valley voltage difference $\hat{X}_s$ (see Fig. 6) of the envelope detector output was selected, the PWD window T_d was optimized and data points were determined for various values of SNR. The table in Fig. 8 lists the demodulator parameters associated with each curve.

As expected the system performance is dependent on the proper selection of threshold V_d. A surprising result is that the value of the threshold voltage V_d which yields the minimum P_e at a given SNR is an approximately constant percentage (32%) of the envelope peak-to-valley voltage difference $\hat{X}_s$. This result is apparently independent of envelope side-lobe level or width of the main lobe. (See column 4 of Table 1.)

Curve of Fig. 9	Content of Filter Output (harmonic number)	Switching Rate (traversals/sec)	$V_d/\hat{X}_s$	Average Pulse Width at Level Detector Output (μsec)	T_d (μsec)
A	1,3,5	12,281	.316	26.0	3.6
B	1,3,5,7	10,647	.325	30.0	7.0
C	1,3,5,7,9	8,419	.318	36.0	7.0
D	-1,1,3,5,7	9,793	.320	45.0	11.5

Table 1 - Summary of parameters of Asynchronous Demodulation System under best performance conditions (Fig. 9).

Data on the performance of the asynchronous demodulator as a function of the number of spectral components in the filter output for PRM by a square wave is presented in Fig. 9. In these experiments the number of the spectral components in the filter output is established

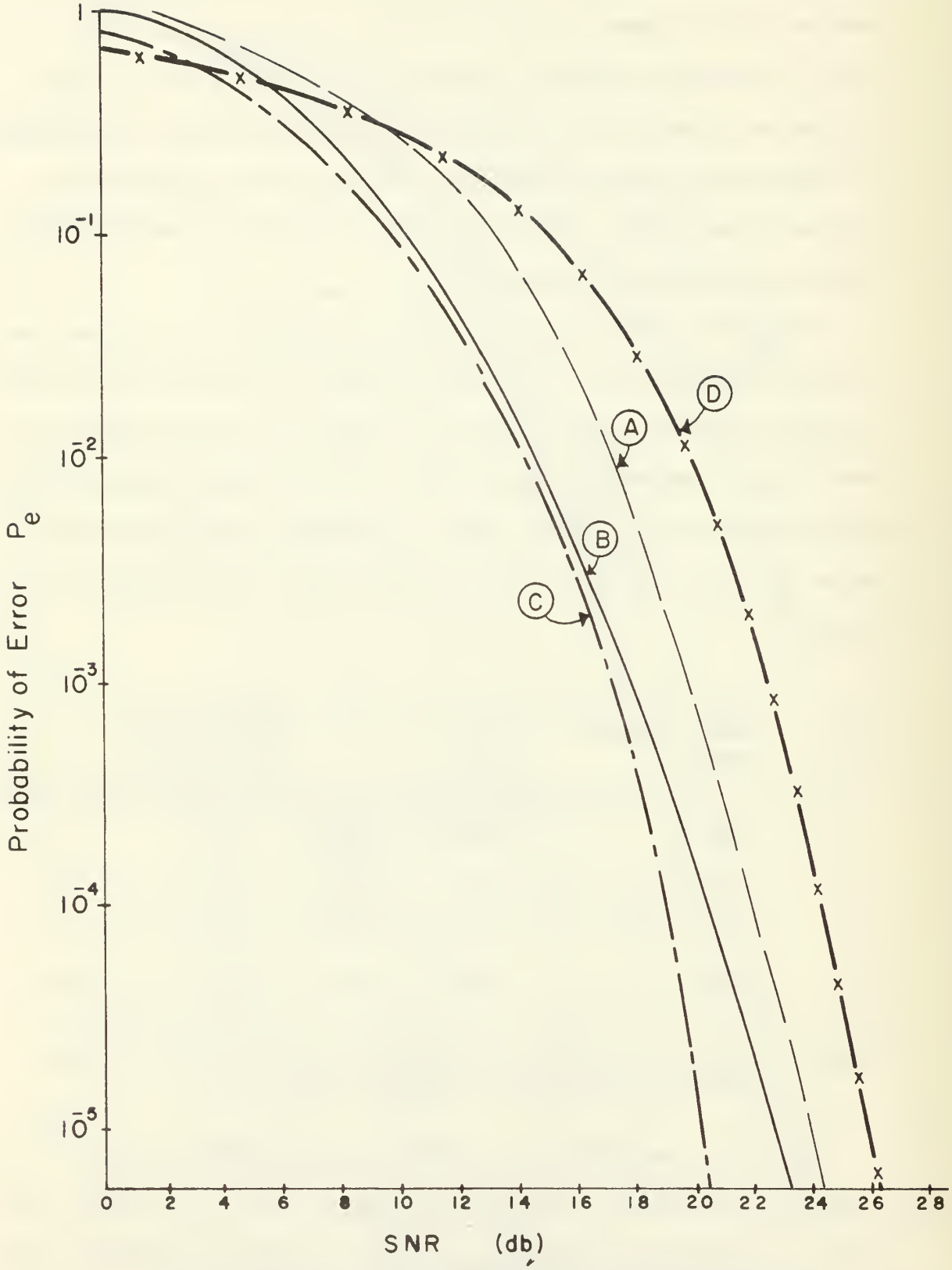

FIG. 9. A PLOT OF THE PERFORMANCE OF AN ASYNCHRONOUS DEMODULATION SYSTEM FOR DIFFERENT NUMBERS OF RETAINED SPECTRAL COMPONENTS. System parameters are adjusted to yield optimum performance as determined experimentally (See Table 1).

by adjusting the switching rate (frequency) of the modulating square-wave. The values of V_d and T_d are adjusted until the minimum P_e is obtained for a SNR of 20 db (measured at the filter output). To obtain the data points, the system parameters were fixed and SNR was varied. As expected, the performance improves as the number of spectral components retained is increased (or for a fixed filter bandwidth, performance improves by reducing the data rate).

Fig. 9 also indicates the degradation in performance resulting from improper filtering of the PRM carrier (curve D). For curve D five side frequencies (first lower and first four upper of PRM by a square-wave) were passed by the filter. Table 1 lists the system parameters for each of the curves of Fig. 9.

In summary, values of the system parameters V_d (expressed as $V_d/\hat{X}_s$) and T_d (expressed as a fraction of the average pulse width (PW) at the output of the level detector) which optimize the performance of the asynchronous demodulation system are $V_d/\hat{X}_s \simeq 0.32$ and $T_d/PW \simeq 0.25$. The pulse width at the output of the threshold detector is approximately the 3 db width of the major lobe of the envelope of the filter output, which is a function of the modulating waveform and filter characteristics (see Fig. 6). The performance of the asynchronous demodulation system as a function of SNR and data rate parallels that of other demodulation systems.

Chapter 3

ANALYSIS

As suggested in Chapter 1, phase-reversal modulation of a carrier is easy to accomplish in practice compared with the generally employed coherent demodulation process. This investigation was motivated by an understanding of the time and frequency descriptions of PRM, both of which suggest the possibility of asynchronously demodulating the PRM carrier with simple circuitry.

From the time-domain description of a PRM carrier it is seen that asynchronous demodulation by using the waveform discontinuity (phase-reversal of the carrier) generated by the changes of state of the binary modulating signal is possible. Differentiation of the PRM carrier will generate voltage spikes at the points of carrier discontinuity; however, as shown in Appendix A this method of detection is not satisfactory because the amplitude of the resulting voltage spike depends on the phase of the carrier at the time of phase reversal. For this reason, this method of asynchronous demodulation is not considered further.

Fourier transform analysis indicates that the spectrum of a periodic pulse-modulated carrier is discrete. As shown in this chapter, if these spectral components are selectively filtered, the resulting waveform is an amplitude-modulated carrier. This phase-modulation to amplitude-modulation (PM to AM) conversion process, used in the experimental procedure, produces major lobes in the envelope of the filtered carrier. These envelope variations are then detected and processed to recover the binary modulating signal.

As shown in this chapter it is generally not possible to analyze completely the performance of the asynchronous demodulation system considered by this study. A statistical analysis or simulation of this

asynchronous demodulation system may be performed with the aid of a digital computer. Such a computer study was not considered in this investigation. Basic analyses of the modulation process and of coherent demodulation of PRM are reviewed. Additionally, an analytical approach to the asynchronous demodulation system of interest here is briefly considered.

A. Phase-Reversal Modulation

A phase-reversal modulated sinusoidal carrier is represented by the expression

$$v(t) = A\cos(\omega_o t + \theta(t)) \tag{1}$$

where A is a constant, ω_o is the carrier frequency in rad/sec and $\theta(t)$ has values 0 and π. An alternate expression for a PRM carrier is

$$v(t) = E(t)[A\cos\ \omega_o t] \tag{2}$$

where the term E(t) is the equivalent of $\cos\ \theta(t)$ and assumes values +1 and -1 when $\theta(t)$ is 0 and π respectively. The spectrum of v(t) is the Fourier transform

$$V(f) = \int_{-\infty}^{\infty} v(t)\exp(-j\omega t)dt = \int_{-\infty}^{\infty} E(t)\cos\ \omega_o t\ \exp(-j\omega t)dt \tag{3}$$

where the constant A is equated to unity here and in the remaining analyses. It is well known [Ref. 2, pp. 322-4] that Eq. (3) reduces to

$$V(f) = \tfrac{1}{2}E(f - f_o) + \tfrac{1}{2}E(f + f_o) \tag{4}$$

where E(f) is the spectrum of the modulating signal given by

$E(f) = \int_{-\infty}^{\infty} E(t)\exp(-j\omega t)dt$. From Eq. (4) it is seen that the carrier spectral term is missing. This conclusion establishes the well-known result that Eq. (2) represents a double-sideband, suppressed carrier, amplitude-modulated signal.

In the experimental work of this investigation, E(t) is a square wave. The time waveform of the square-wave modulated carrier is given by

$$v(t) = \sum_{n=1}^{\infty} \frac{\sin[(2n-1)\,\pi/2]}{(2n-1)\,\pi/2} \{\cos[\omega_o - (2n-1)\omega_m]t - \cos[\omega_o + (2n-1)\omega_m]t\} \tag{5}$$

For the case of PRM by a square-wave, the modulated-carrier spectrum is

$$V(f) = \sum_{n=1}^{\infty} \frac{\sin[(2n-1)\pi/2]}{(2n-1)\pi/2} \left[\delta\{f - [f_o - (2n-1)f_m]\} - \delta\{f - [f_o + (2n-1)f_m]\}\right] \tag{6}$$

where V(f) is the one-sided spectrum and f_m is the fundamental frequency of the square-wave modulating signal. In Eq. (6), $\delta(x)$ is the ordinary Dirac delta function having a value of unity when its argument x is zero and a value of zero elsewhere. For E(t) a square wave, v(t) and its spectrum V(f) are as shown in Figs. 10b and 10c respectively. If E(t) is not periodic, i.e., a random two-level signal, then the modulated carrier spectrum V(f) is continuous rather than discrete. Bennett [Ref. 2, pp. 315-21] presents an interesting probabilistic analysis of the time waveform and the spectrum of a carrier modulated by a random binary signal. His analysis, applicable to PRM, assumes the encoding system in use provides a fixed probability of a mark and space occurring. The results of Bennett's analysis are in the same form as Eqs. (2) and (4) except that the terms are weighted with the specific probabilities of occurrence of each level of E(t).

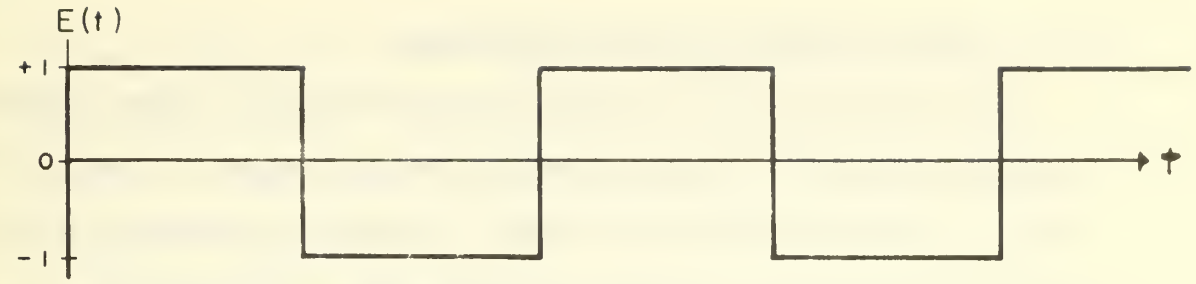

(a) Modulating waveform E(t).

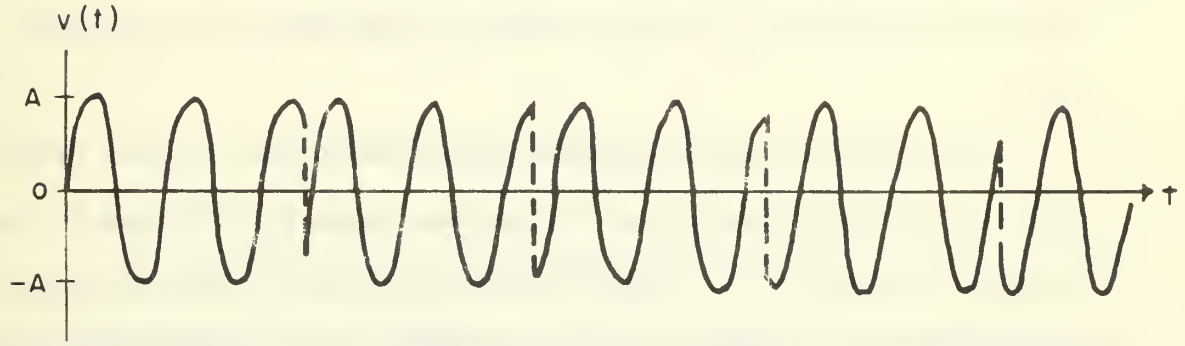

(b) PRM carrier time waveform v(t).

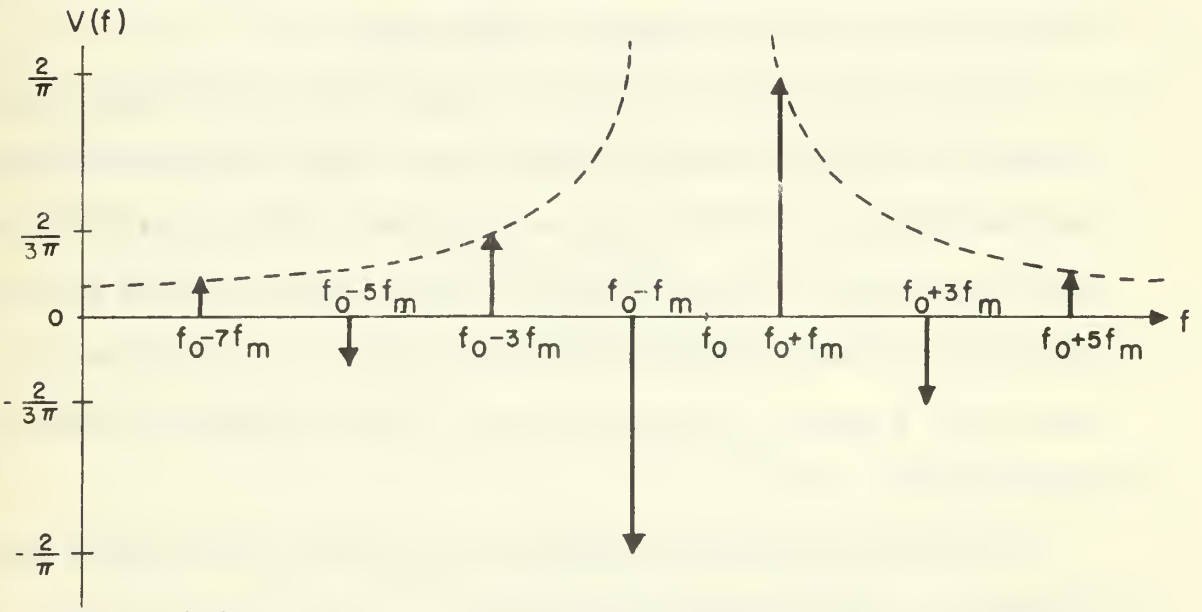

(c) PRM carrier one-sided spectrum.

FIG. 10. ILLUSTRATION OF THE TIME AND FREQUENCY DESCRIPTIONS OF A CARRIER PHASE-REVERSAL MODULATED BY A SQUARE WAVE.

B. Coherent Demodulation of a PRM Carrier

The various methods of coherent demodulation of a phase-reversal modulated signal have been analyzed by various authors. Three basic types of coherent demodulation emerge: coherent, differentially coherent and partially coherent. In coherent detection of PRM the unmodulated carrier frequency and phase are known exactly. As a result coherent detection is optimum in the sense that it provides the lowest probability of error P_e for all values of SNR [Ref. 2, pp. 210-20; Ref. 5].

In the differentially coherent detection system the data (switching) rate is known exactly and the carrier phase is estimated by comparing the signal of the present switching interval with the signal of the immediately preceding switching interval. The differentially coherent detection system suffers a one db degradation in performance relative to the coherent detection system [Ref. 4].

The partially coherent detection system uses a phase-locked loop to derive the local reference from the input signal, typically by using the loop feed back (error) signal as a measure of the variation of the input signal phase. The performance of this detection system approaches that of the optimum coherent detection system, but the operation is a function of a number of variables each of which can degrade performance [Ref. 6].

The minimum attainable probability of error P_e for a binary data transmission system has been shown to be

$$P_e = \frac{1}{2}(1 - \text{erf}\sqrt{E/N_o}) \tag{7}$$

where E is the signal energy per bit and N_o the noise power per Hz of band width [Ref. 4]. The term E is calculated by multiplying the average

carrier signal power by the fundamental switching interval T_m of the modulating waveform. For pure PRM the envelope is a constant A and the power in the signal relative to a one-ohm resistor is $A^2/2$ (or $E = T_m/2 = 1/2f_m$ for $A = 1$).

To compare the band-limited asynchronous demodulation system with the coherent system, it is necessary to determine the effect of band-limiting on the performance of the coherent system. The average power of the PRM signal is calculated by [Ref. 7, pp. 267-82]

$$P_{avg} = \frac{1}{T_m} \int_o^{T_m} v(t)^2 dt \tag{8}$$

For a square-wave modulated PRM carrier, v(t) and V(f) are given by Eqs. (5) and (6) respectively. For the case of four spectral components in the pass band of the filter Eq. (8) gives $P_{avg} \simeq .45A^2$. The energy per bit of the band-limited PRM carrier is about 90% of that of the unfiltered PRM carrier or about -.46 db less. If it is assumed that the noise spectrum is a constant N_o the degradation in performance of the coherent system due to band limiting is approximately 0.5 db. Therefore, the optimum performance curve of Fig. 5 is shifted to the right about 0.5 db to give the performance of the filtered (4 side-frequency case) PRM carrier.

For the case of a 50 kHz pass band containing exactly four spectral components (square-wave modulation) the maximum and minimum switching rates are 12.5 kHz and 8.4 kHz respectively. An additional degradation factor of 8.4/12.5 or up to 1.65 db could occur due to improper utilization of the filter passband; i.e., the 8.4 kHz switching rate permits a greater total noise power without increasing the signal power appearing at the fixed bandpass filter output, whereas

the 12.5 kHz data rate utilizes all of the filter passband.

In the experiment a switching rate of 10.6 kHz was used. For the four spectral component case, Fig. 11 shows the optimum detection curve of Fig. 5 displaced horizontally to the right by 1.7 db. This displacement accounts for practical performance (-0.5 db), band limiting power loss (-0.5 db) and band utilization loss (-0.7 db). In Fig. 11 the asynchronous demodulation system experimental performance curve for the bandlimited case (four side frequencies retained) is also shown for comparison.

C. Asynchronous Demodulation of a PRM Carrier

Filtering the PRM carrier results in an amplitude-modulated carrier. The form of the envelope of the filtered PRM carrier depends on the type of filtering used. Using the expression of PRM by a square wave given in Eq. (5), Cumming [Ref. 8] noted that if only those frequency components of the spectrum above the carrier frequency f_o are present in the output of a highpass filter (single side band filtering or positive integer values of n in Eq. (5)) the resultant time waveform will have spikes approaching infinite amplitude at the points of phase-reversal. This may be seen by considering Eq. (5) after rewriting it to account for the high pass filtering

$$v_u(t) = \sum_{n=1}^{\infty} \frac{\sin[(2n-1)\,\pi/2]}{(2n-1)\,\pi/2} \{\cos[\omega_o + (2n-1)\omega_m]t\} \qquad (9)$$

Since $v_u(t)$ is periodic with period $2\,\pi/\omega_m$ and since

$$v_u(0) = \sum_{n=1}^{\infty} \frac{2}{\pi(2n-1)} = \infty$$

then $v_u(t)$ assumes values of infinity whenever the unfiltered carrier v(t) changes phase. It is obvious from Fig. 12 that the modulating

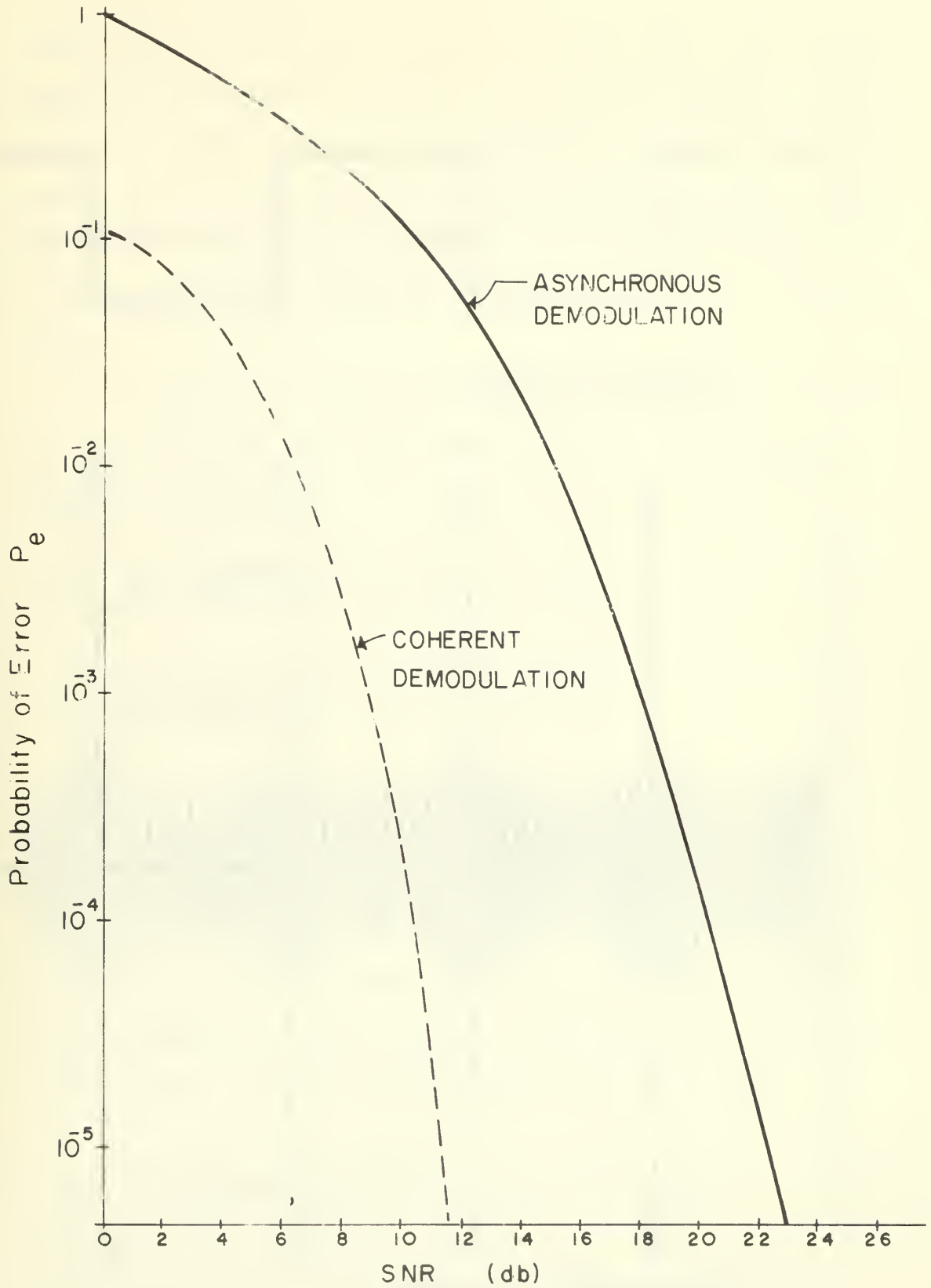

FIG. 11. A COMPARISON OF THE PERFORMANCE OF COHERENT AND ASYNCHRONOUS DEMODULATION SYSTEMS. The carrier is phase-reversal modulated by a square wave. Four spectral components of the filtered carrier are retained.

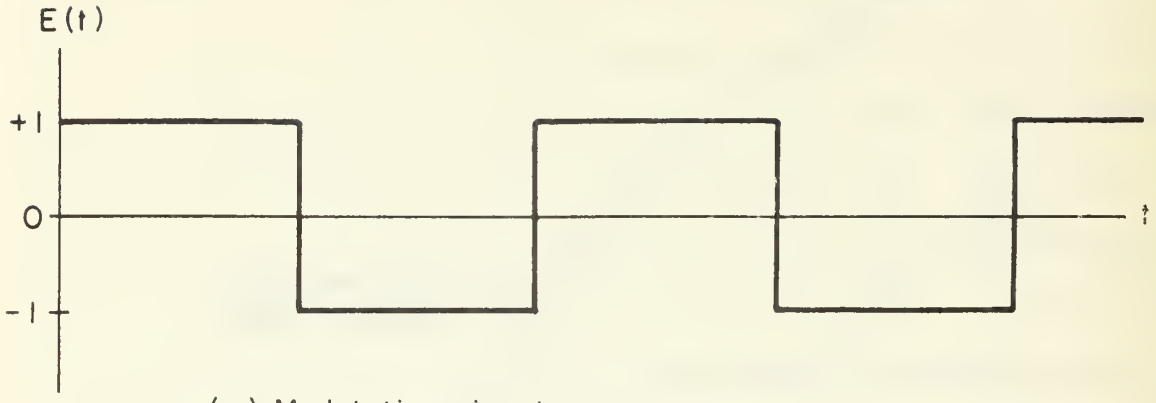

(a) Modulating signal.

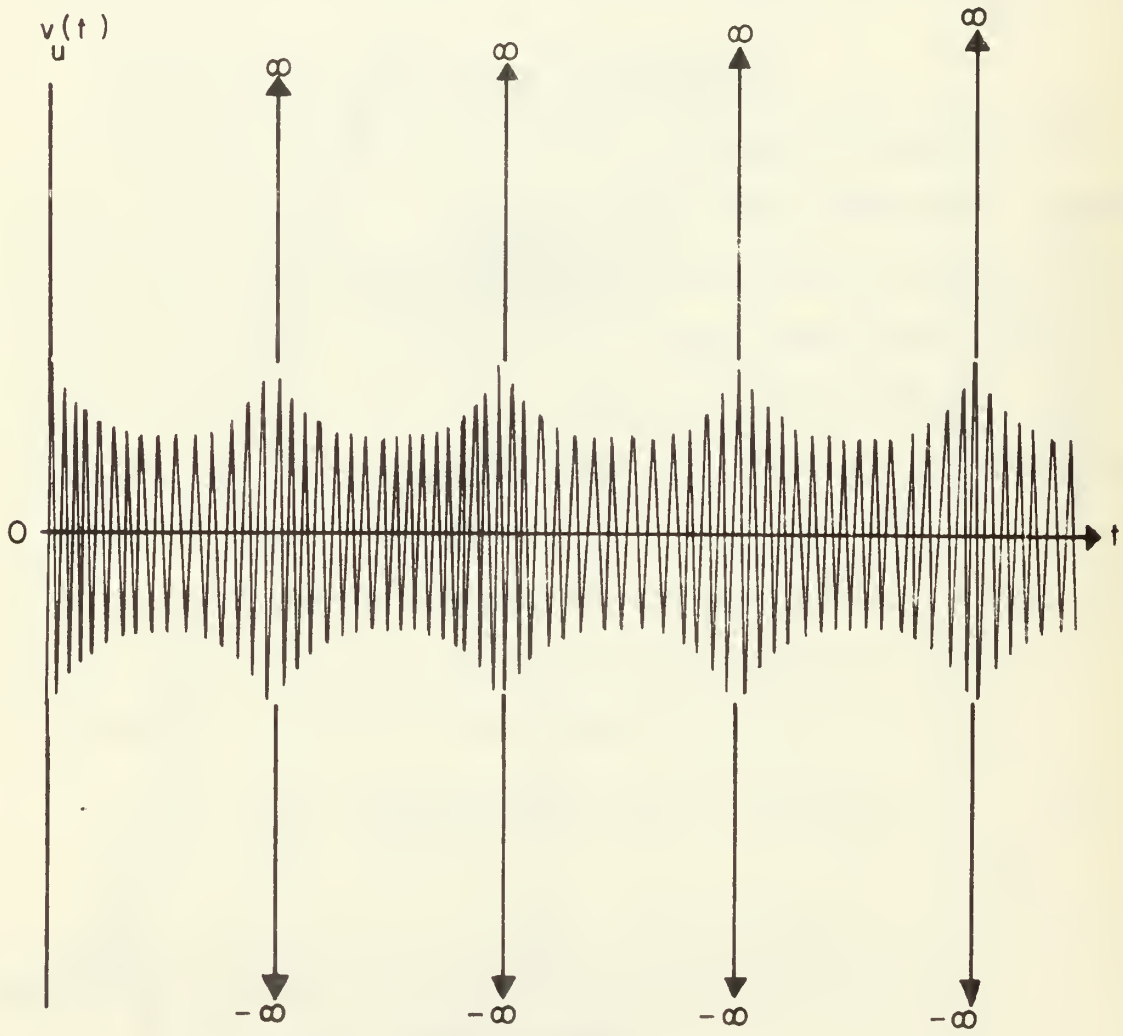

(b) Highpass filter output.

FIG. 12. AN ILLUSTRATION OF THE WAVEFORM OBTAINED BY REMOVING THE LOWER-SIDE-FREQUENCY COMPONENTS OF A CARRIER PHASE-REVERSAL MODULATED BY A SQUARE WAVE.

waveform E(t) can be simply recovered from $v_u(t)$ with a threshold detector and modest logic circuitry. In practice it is neither possible because of transmitter filtering, nor desirable because of the noise problem, to retain many of the frequency components of v(t). Therefore, it is the purpose of this study to determine the suitability of a "narrowband" filter - threshold detector combination as a demodulator system.

For the case of a carrier phase-reversal modulated by a square wave and filtered by an "ideal" bandpass filter, the filter output $v_f(t)$ is, using Eq. (5)

$$v_f(t) = \sum_{n=i}^{k} \frac{\sin[(2n-1)\,\pi/2]}{(2n-1)\,\pi/2} \{\cos[\omega_o - (2n-1)\omega_m]t\} \tag{11a}$$

$$= \sum_{n=i}^{k} \frac{\sin[(2n-1)\,\pi/2]}{(2n-1)\,\pi/2} [\cos(2n-1)\omega_m t]\cos\omega_o t$$

$$+ \sum_{n=i}^{k} \frac{\sin[(2n-1)\,\pi/2]}{(2n-1)\,\pi/2} [\sin(2n-1)\omega_m t]\sin\omega_o t \tag{11b}$$

$$= R(t)\cos\omega_o t + S(t)\sin\omega_o t \tag{11c}$$

The lower limit i and the upper limit k of the indexing integer n are determined by the lower and upper cutoff frequencies respectively of the filter. The one-sided spectrum of $v_f(t)$ of Eq. (11) is

$$V_f(f) = \sum_{n=i}^{k} \frac{\sin[(2n-1)\,\pi/2]}{(2n-1)\,\pi/2} [\delta\{f - [f_o - (2n-1)f_m]\}] \tag{12}$$

Fig. 13 shows the one-sided spectrum of the bandpass filter output $v_f(t)$ for the case of PRM by a square wave (compare with Fig. 10c).

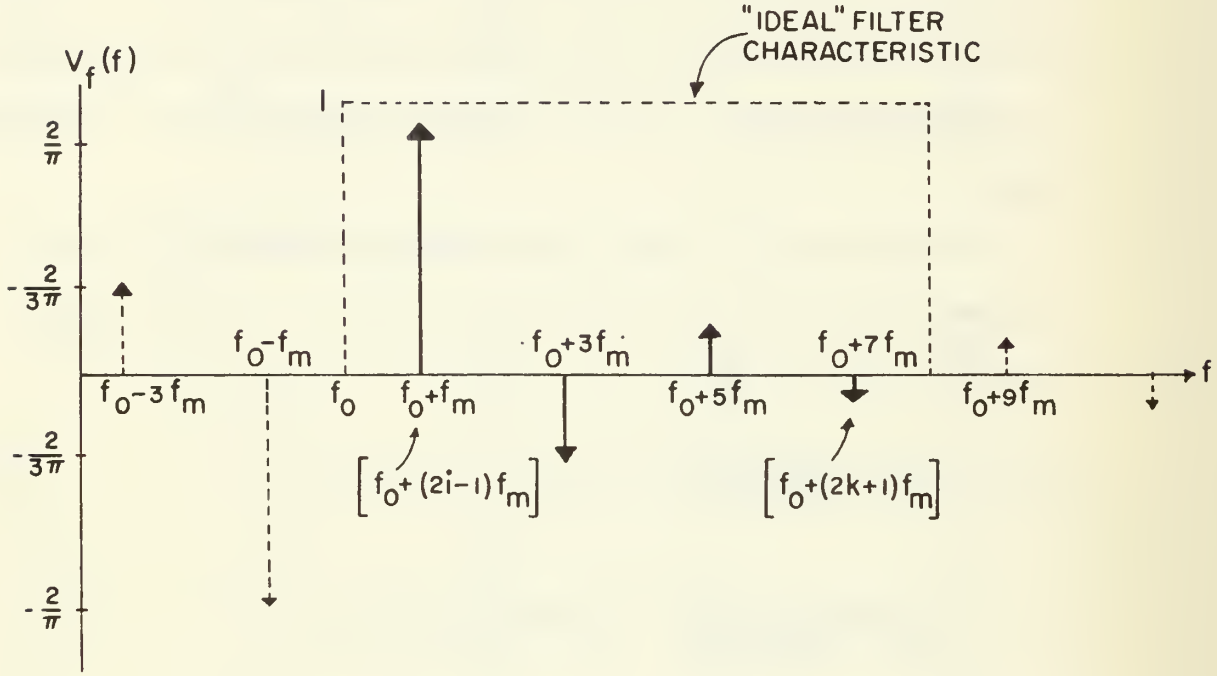

FIG. 13. AN EXAMPLE OF THE ONE-SIDED SPECTRUM OF THE OUTPUT OF A BANDPASS FILTER EXCITED BY A CARRIER PHASE-REVERSAL MODULATED BY A SQUARE WAVE.

The envelope $X_s(t)$ of the filtered time waveform of Eq. (11) is given by

$$X_s(t) = \sqrt{R^2(t) + S^2(t)} \tag{13}$$

where R(t) and S(t) are defined in Eq. (11c).

Using Eq. (13) a number of computer calculations were made to determine the envelope of a square-wave-modulated PRM carrier after bandpass filtering. The results where only the upper (above f_o) spectral components are passed by the filter (n in Eq. (11) takes on positive integer values) are considered first. These results are mathematically the same if the same number of the lower spectral components are passed

by the filter. Figs. 14a, b, c, d, e and f show the resulting envelope for 3, 4, 5, 10, 25 and 50 spectral components respectively. Figs. 14a, b and c additionally show the envelope obtained experimentally.

The two envelope characteristics of importance for AM detection are the peak-to-valley ratio of the envelope and the width of the major lobe which occurs each time the carrier phase is switched. Fig. 15 shows the envelope peak-to-valley ratio in db (10 log V_{max}/V_{min}) as a function of the number of spectral components passed by the filter. It is seen that the peak-to-valley ratio does not increase appreciably as the number of side frequencies (filter pass band for fixed f_m) is increased. This is to be expected since the amplitude of the n^{th} spectral component in the square-wave modulated case is $2/[(2n-1)\pi]$ and slightly more than 99% of the signal power is contained in the first ten spectral components.

Fig. 16 indicates the pulse width (half power points) of the envelope as a function of the number of spectral components for PRM by a square wave. As shown in Fig. 16, the pulse width decreases as the number of side frequencies increases. With ten spectral components in the filter passband, the pulse width is 6% of the switching interval. It appears, therefore, that ten or less spectral components in the square wave modulation case are adequate in a practical system. Hence, the bandwidth of the filter need be no greater than $19f_m$, where f_m is the fundamental frequency of the modulating square wave. In practice, as few as four spectral components will provide satisfactory performance as shown by this study.

The envelope of a filtered carrier PRM by a square wave was determined with the aid of a computer for a number of cases where the spectrum of the filter output was not limited to upper spectral

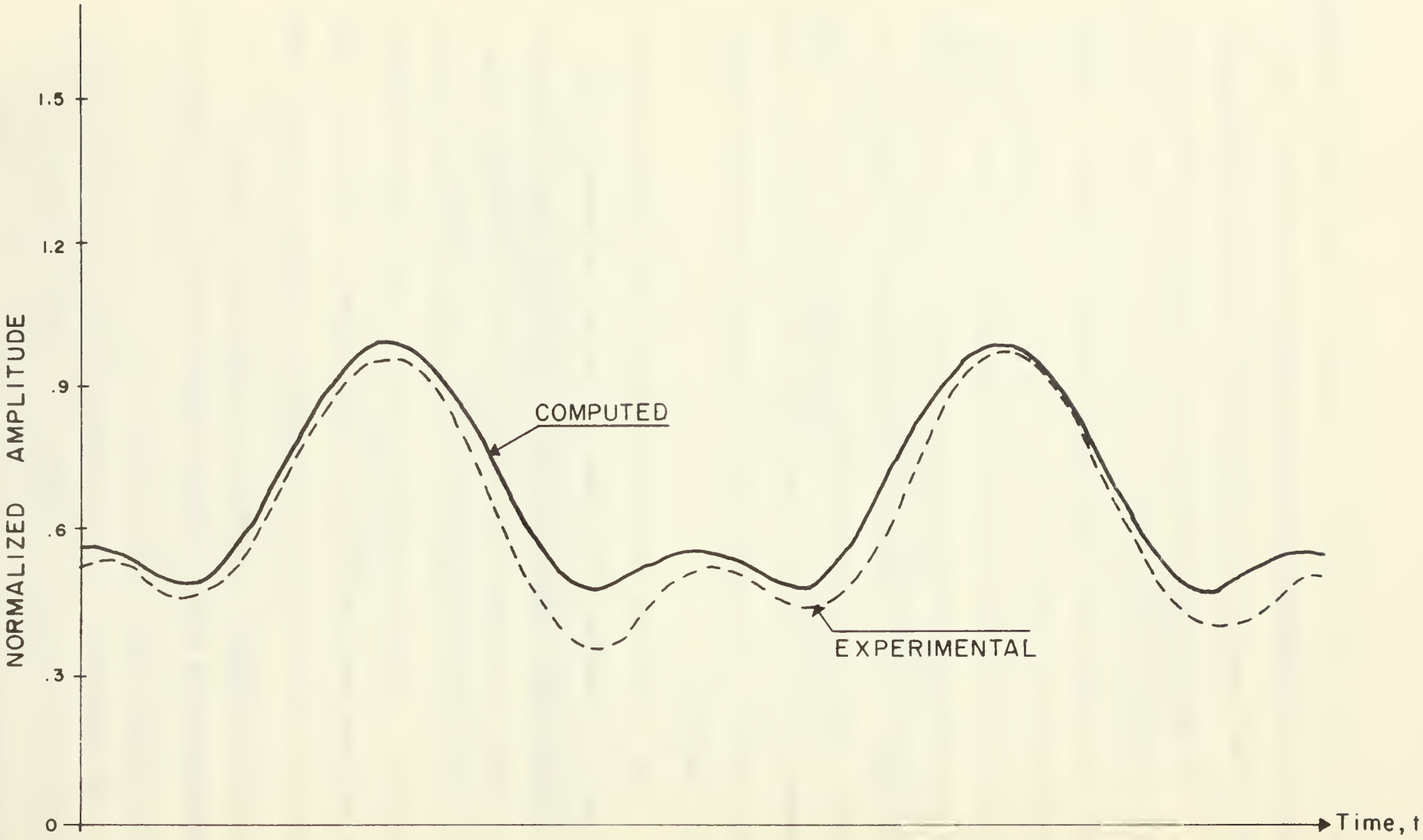

FIG. 14a. EXAMPLES OF THE ENVELOPE OF THE OUTPUT OF THE PM-TO-AM CONVERTER (BANDPASS FILTER). The carrier is phase-reversal modulated by a square wave. Three spectral components are retained by the filter.

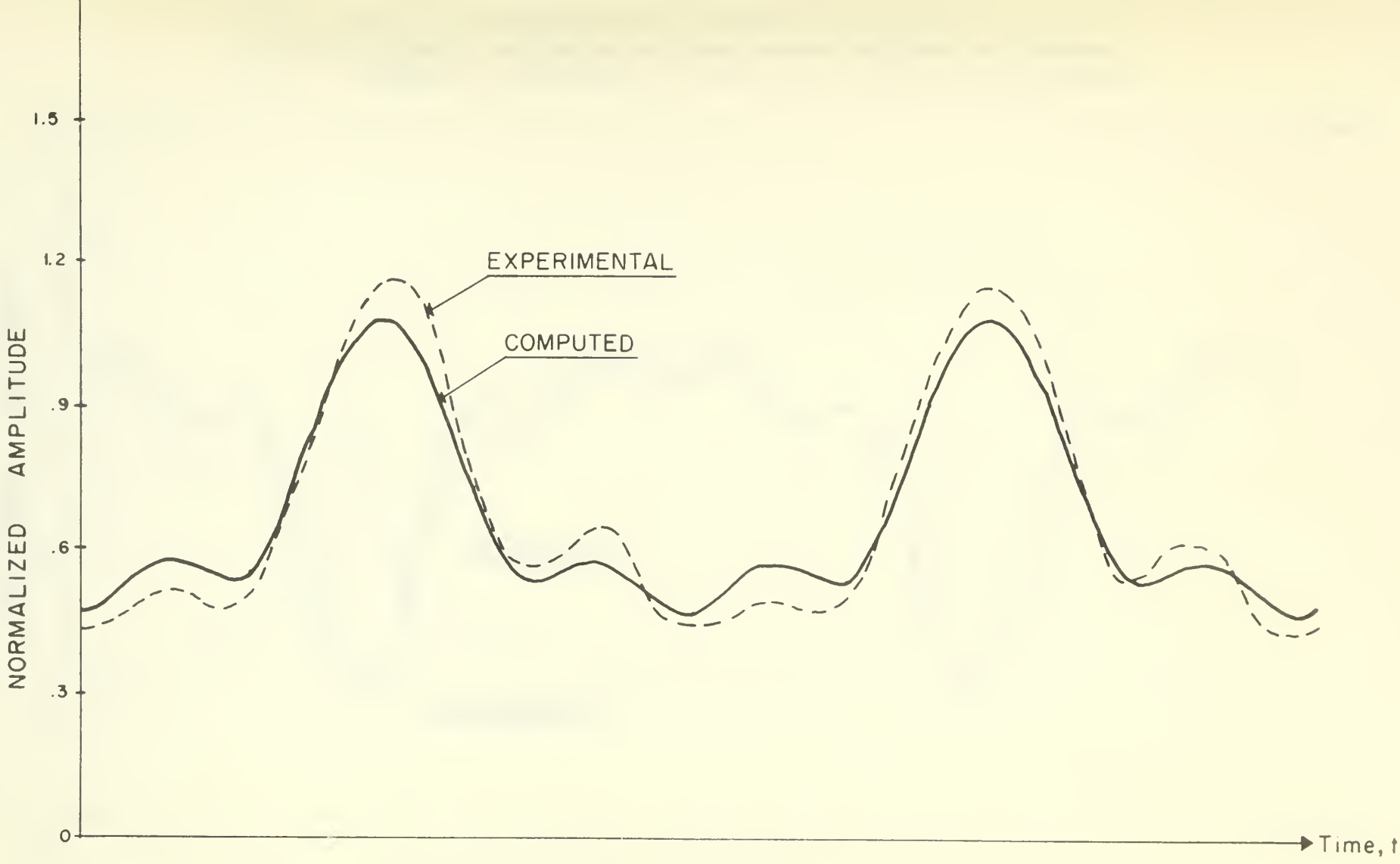

FIG. 14b. EXAMPLES OF THE ENVELOPE OF THE OUTPUT OF THE PM-TO-AM CONVERTER (BANDPASS FILTER). The carrier is phase-reversal modulated by a square wave. Three spectral components are retained by the filter.

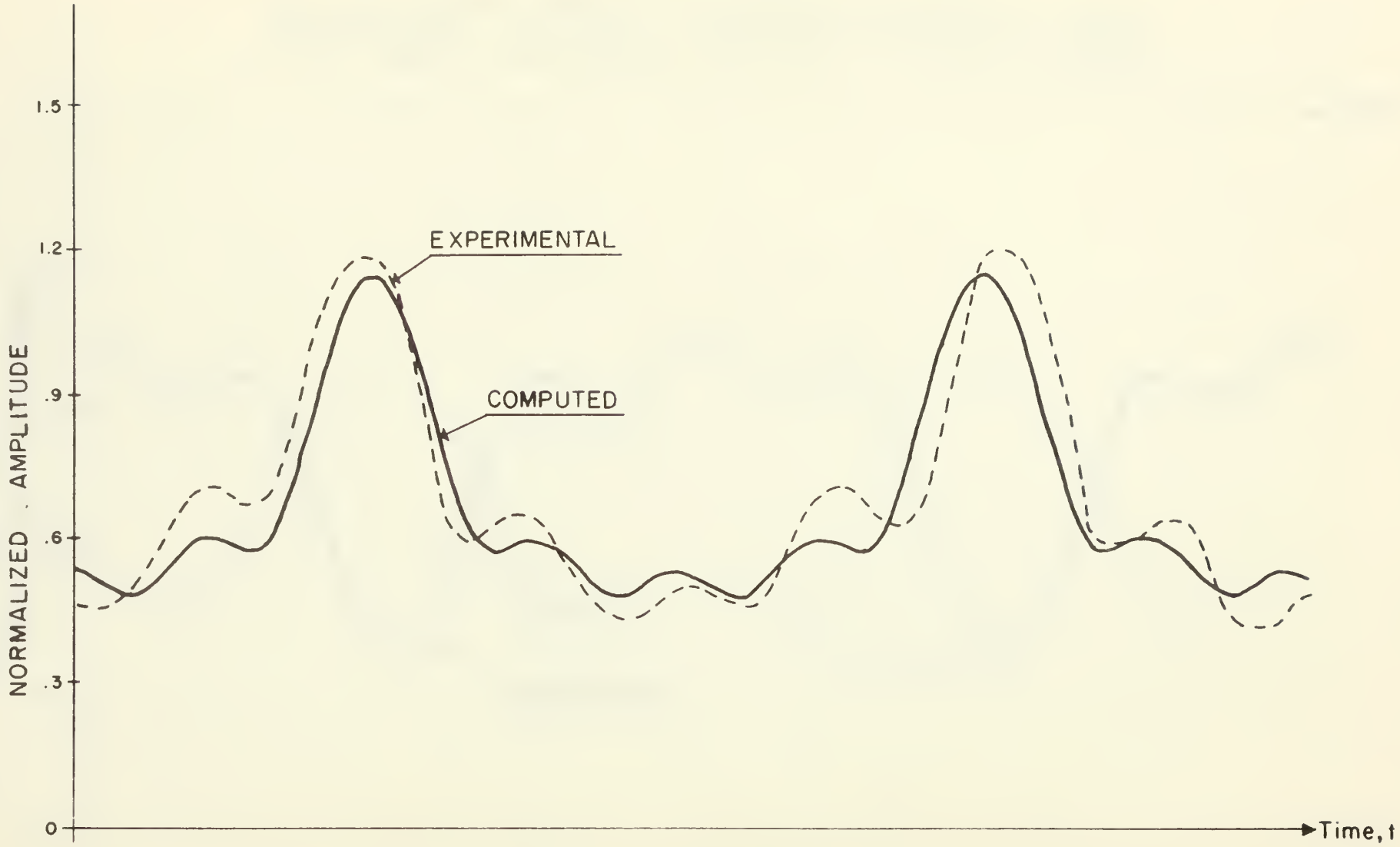

FIG. 14c. EXAMPLES OF THE ENVELOPE OF THE OUTPUT OF THE PM-TO-AM CONVERTER (BANDPASS FILTER). The carrier is phase-reversal modulated by a square wave. Five spectral components are retained by the filter.

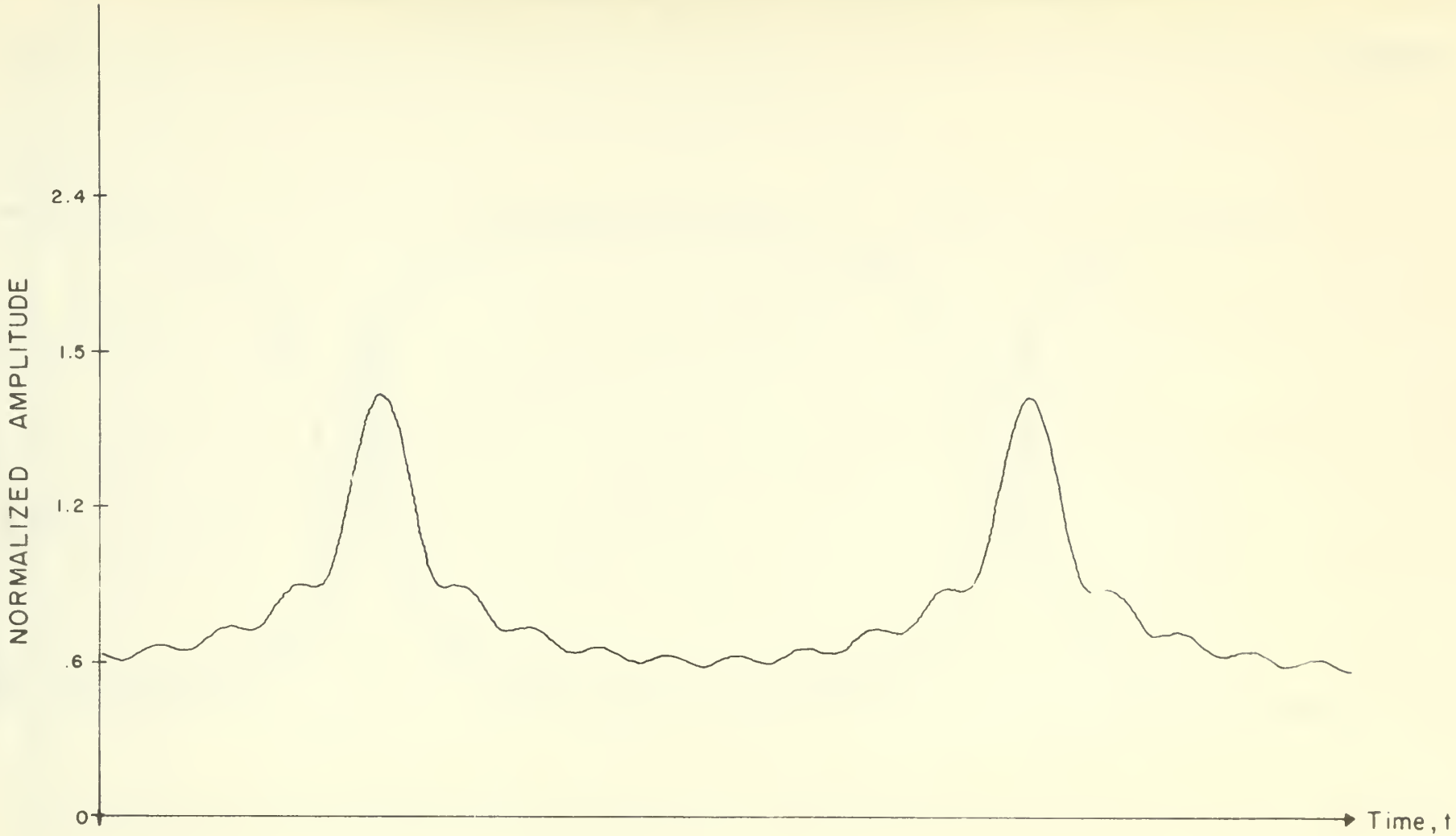

FIG. 14d. EXAMPLE OF THE ENVELOPE OF THE OUTPUT OF THE PM-TO-AM CONVERTER (BANDPASS FILTER). The carrier is phase-reversal modulated by a square wave. Ten spectral components are retained by the filter.

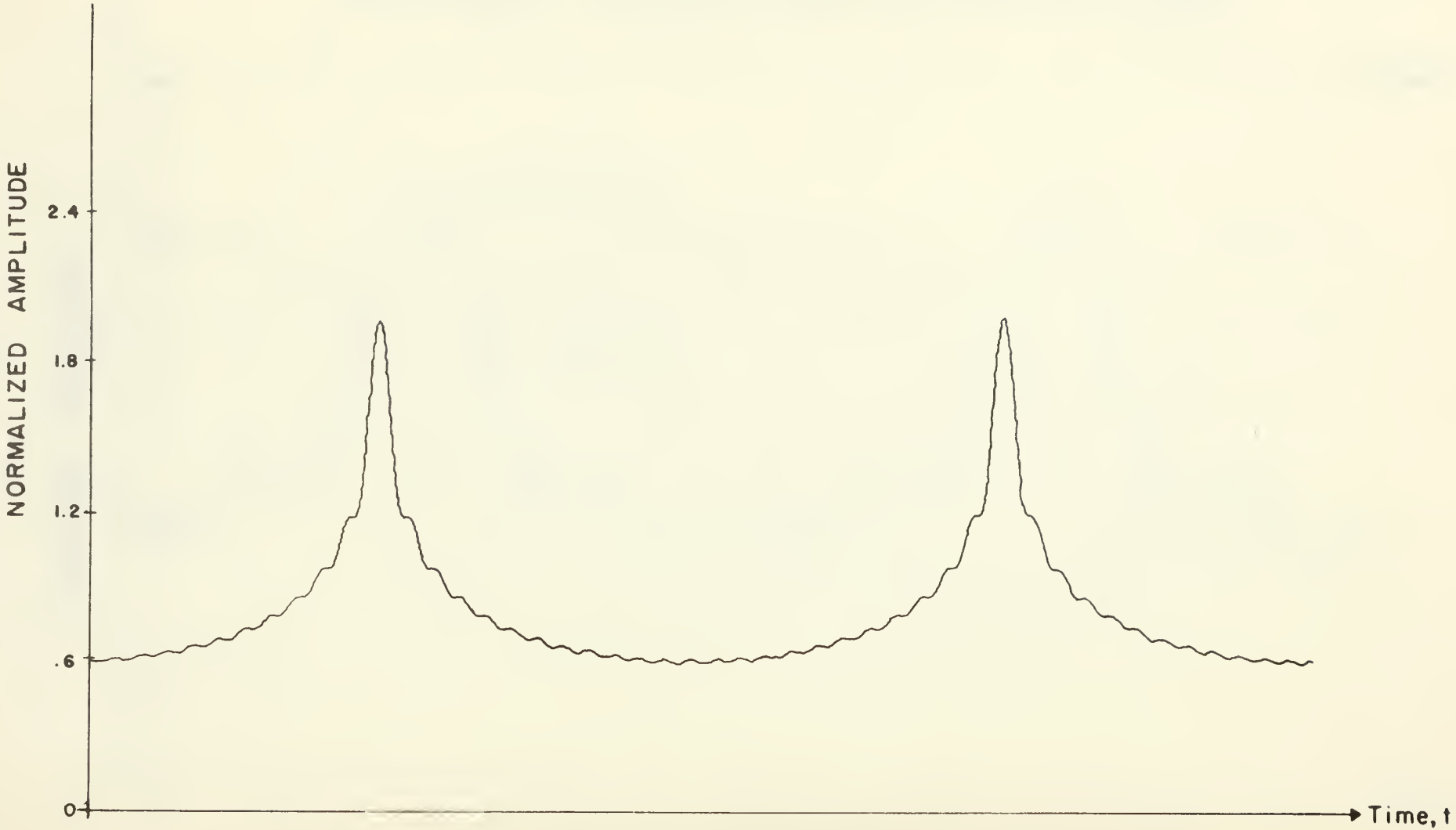

FIG. 14e. EXAMPLE OF THE ENVELOPE OF THE OUTPUT OF THE PM-TO-AM CONVERTER (BANDPASS FILTER). The carrier is phase-reversal modulated by a square wave. Twenty five spectral components are retained by the filter.

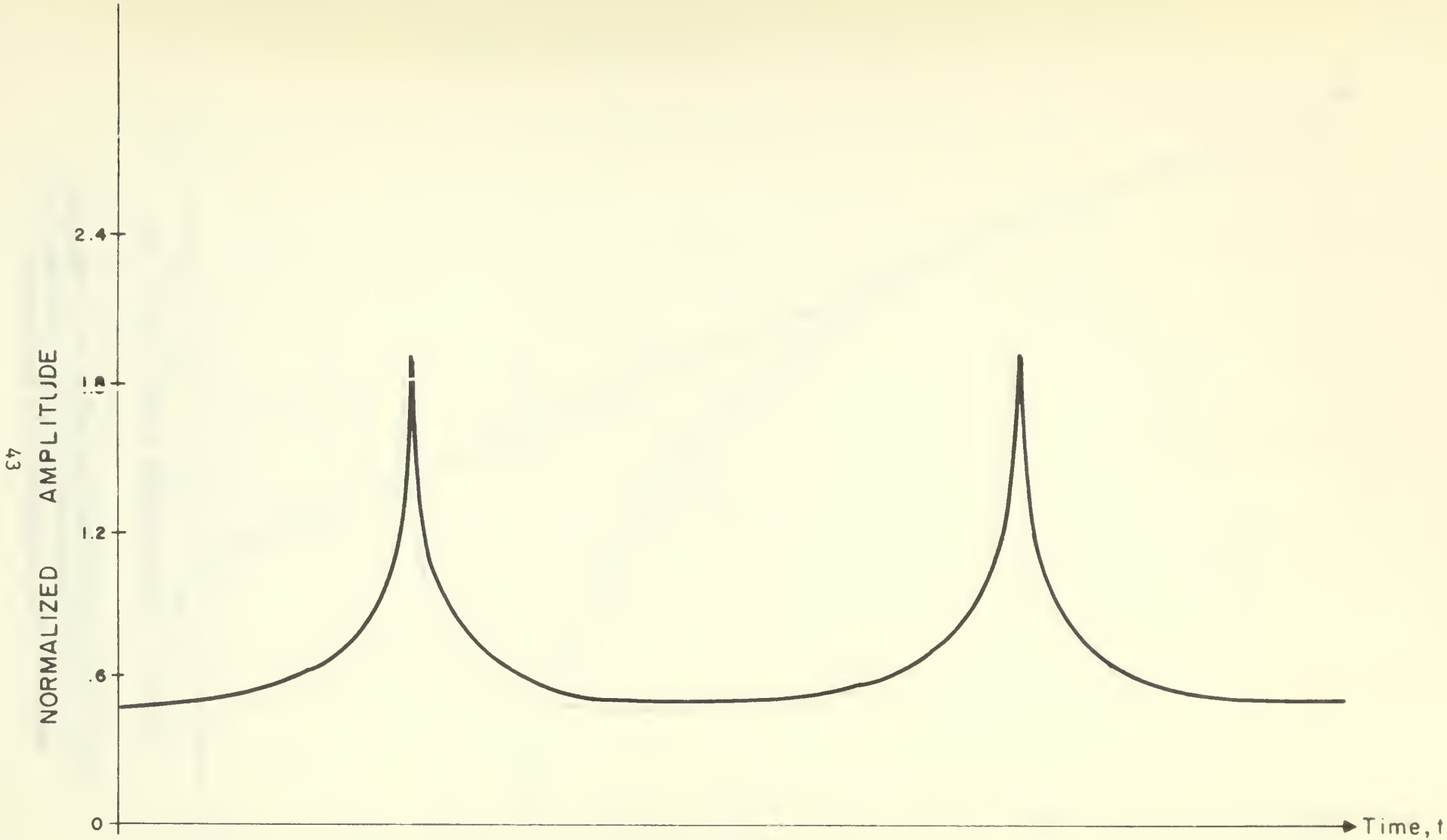

FIG. 14f. EXAMPLE OF THE ENVELOPE OF THE OUTPUT OF THE PM-TO-AM CONVERTER (BANDPASS FILTER). The carrier is phase-reversal modulated by a square wave. Fifty spectral components are retained by the filter. The fine structure of the envelope does not show.

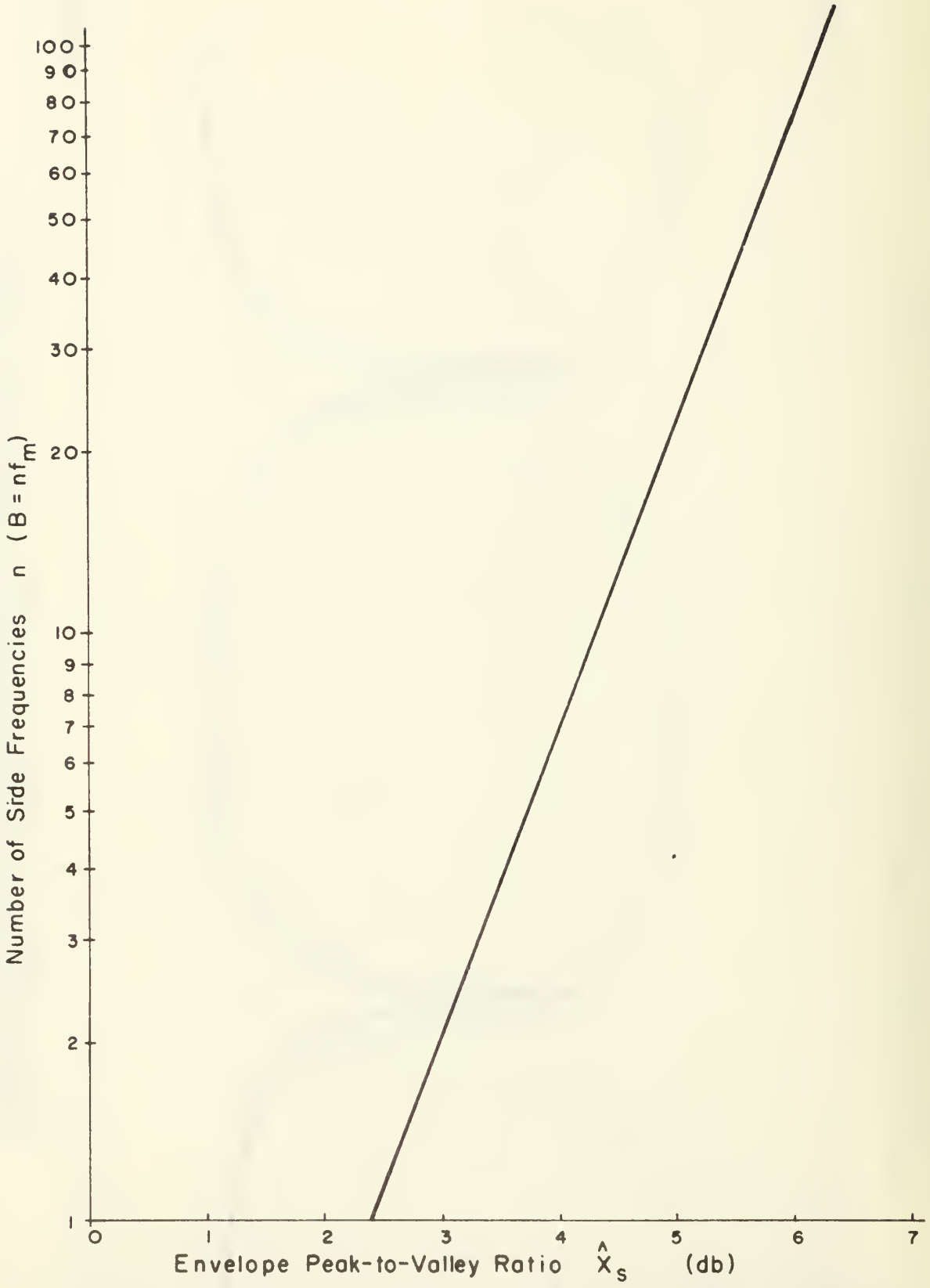

FIG. 15. A PLOT OF THE NUMBER OF SIDE FREQUENCIES VS ENVELOPE PEAK-TO-VALLEY RATIO. The carrier is phase-reversal modulated by a square wave.

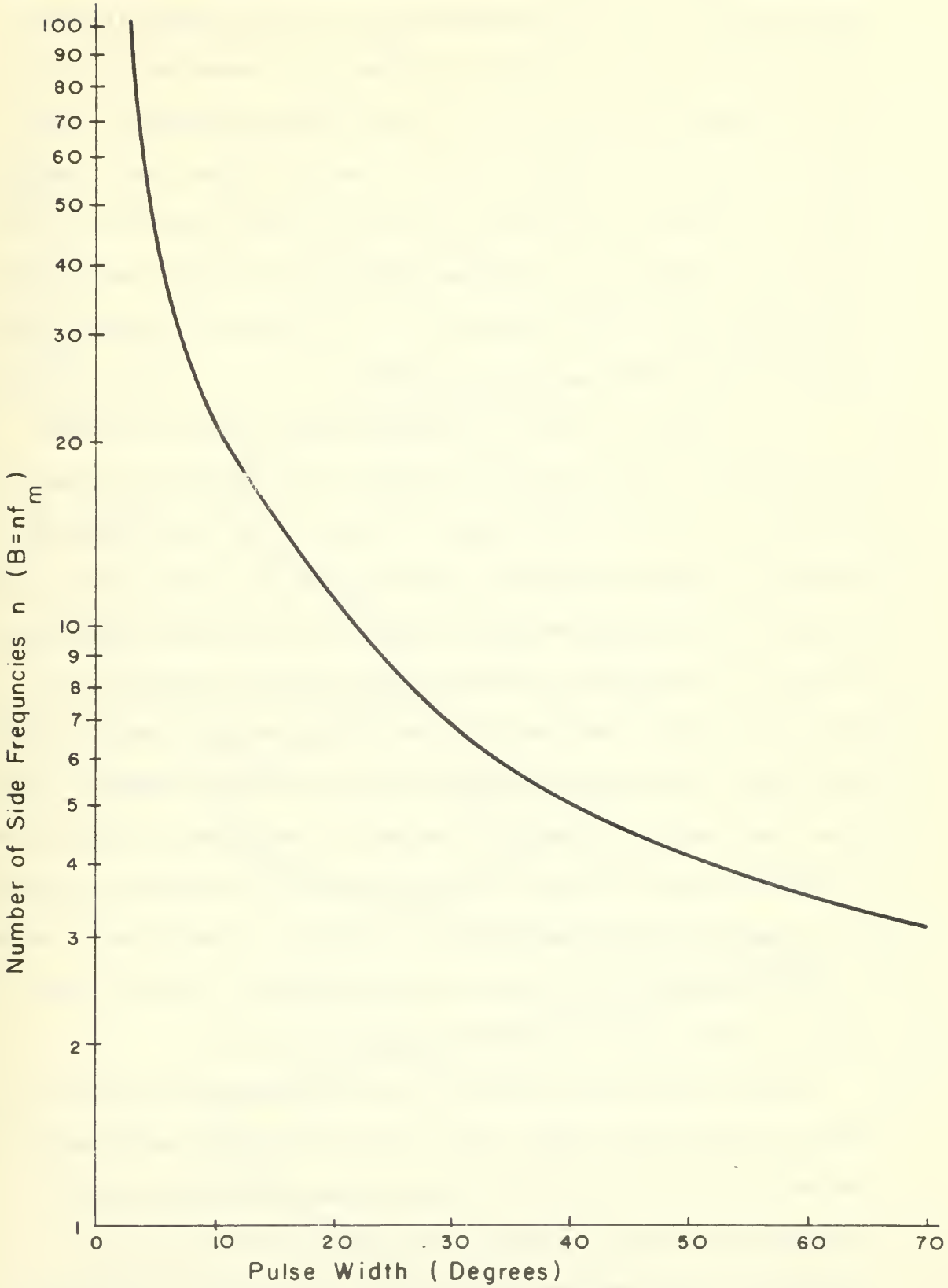

FIG. 16. A PLOT OF THE NUMBER OF SIDE FREQUENCIES VS WIDTH OF THE ENVELOPE MAJOR LOBE. The carrier is phase-reversal modulated by a square wave.

components only. Fig. 17 shows the resulting envelope when four spectral components are taken symmetrically about the carrier frequency (the first two upper and first two lower side frequencies) in curve A. The calculated envelope of the four upper side frequencies is also shown in curve B. As shown in Fig. 17 the major lobes that formerly occur at the switching times of the carrier phase become nulls. For the case of symmetrical filtering, the envelope flattens between the switching points and the nulls narrow as the number of spectral components in the filter pass band increase.

Fig. 18 shows a family of calculated envelopes of a filtered carrier PRM by a square wave with eight of the upper side frequencies included in the filter pass band. For curve A the first eight side frequencies (above the carrier) are included. For curve B the spectrum consists of the second through the ninth side frequencies simulating the case of a bandpass filter whose lower cutoff frequency is too large. For curve C the spectrum consists of the first lower and first eight upper side frequencies simulating the case of a bandpass filter whose lower cutoff frequency is too small. Comparison of curves A and C shows that curve C begins to take the form of the envelope resulting from symmetrical filtering (curve A of Fig. 17). Comparison of curves A and B shows the shape factors to be approximately the same; the loss of signal power is evident, however, in curve B.

Having established the form of the envelope resulting from filtering the PRM carrier (Eq. (13)), we now consider the performance of the AM detection portion of the asynchronous demodulation system. As indicated by Fig. 19, with a fixed threshold level V_d, each occurrence of the envelope exceeding the threshold V_d is passed by

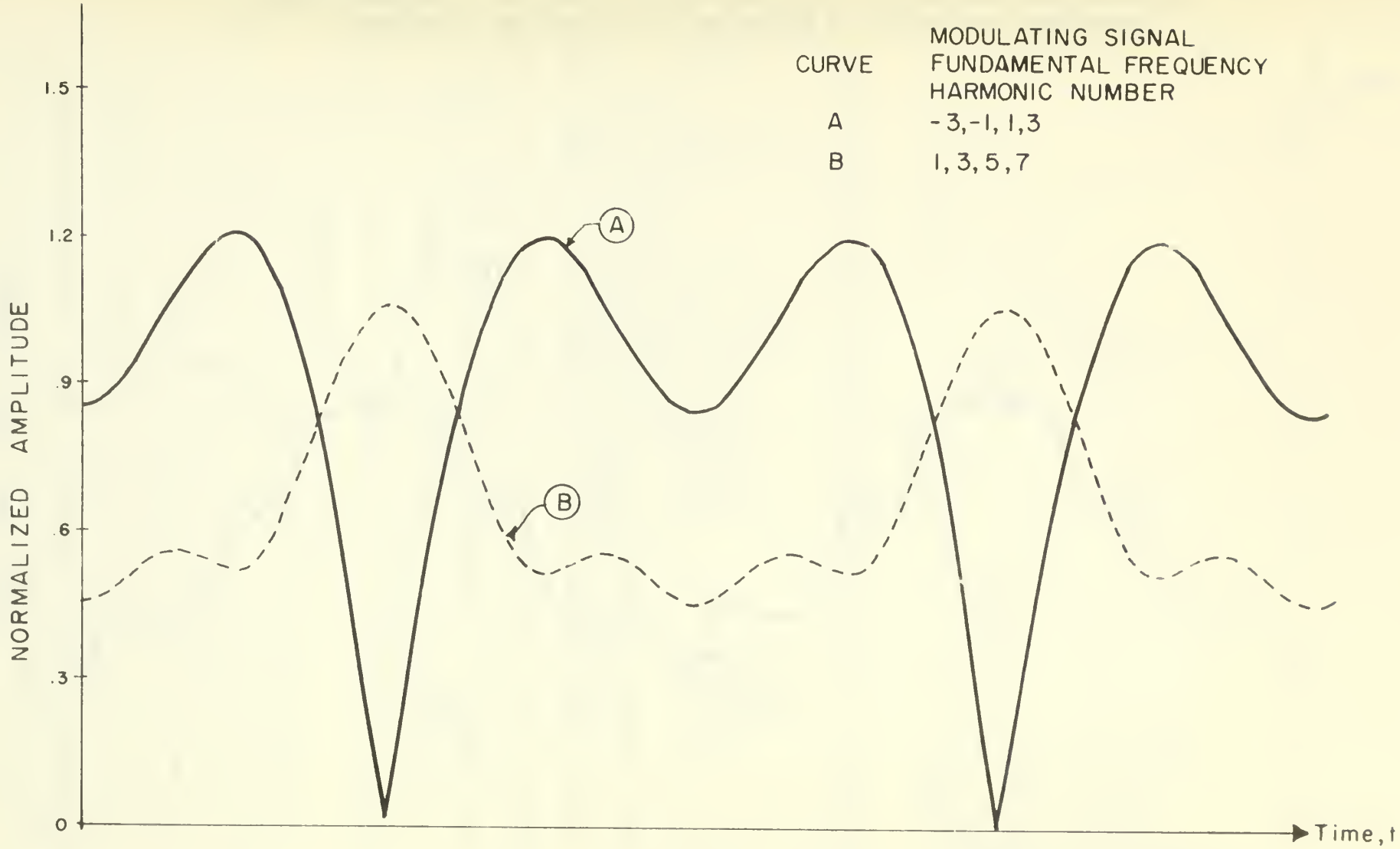

FIG. 17. EXAMPLES OF THE ENVELOPE OF THE OUTPUT OF THE PM-TO-AM CONVERTER (BANDPASS FILTER). Two sets of four spectral components are considered.

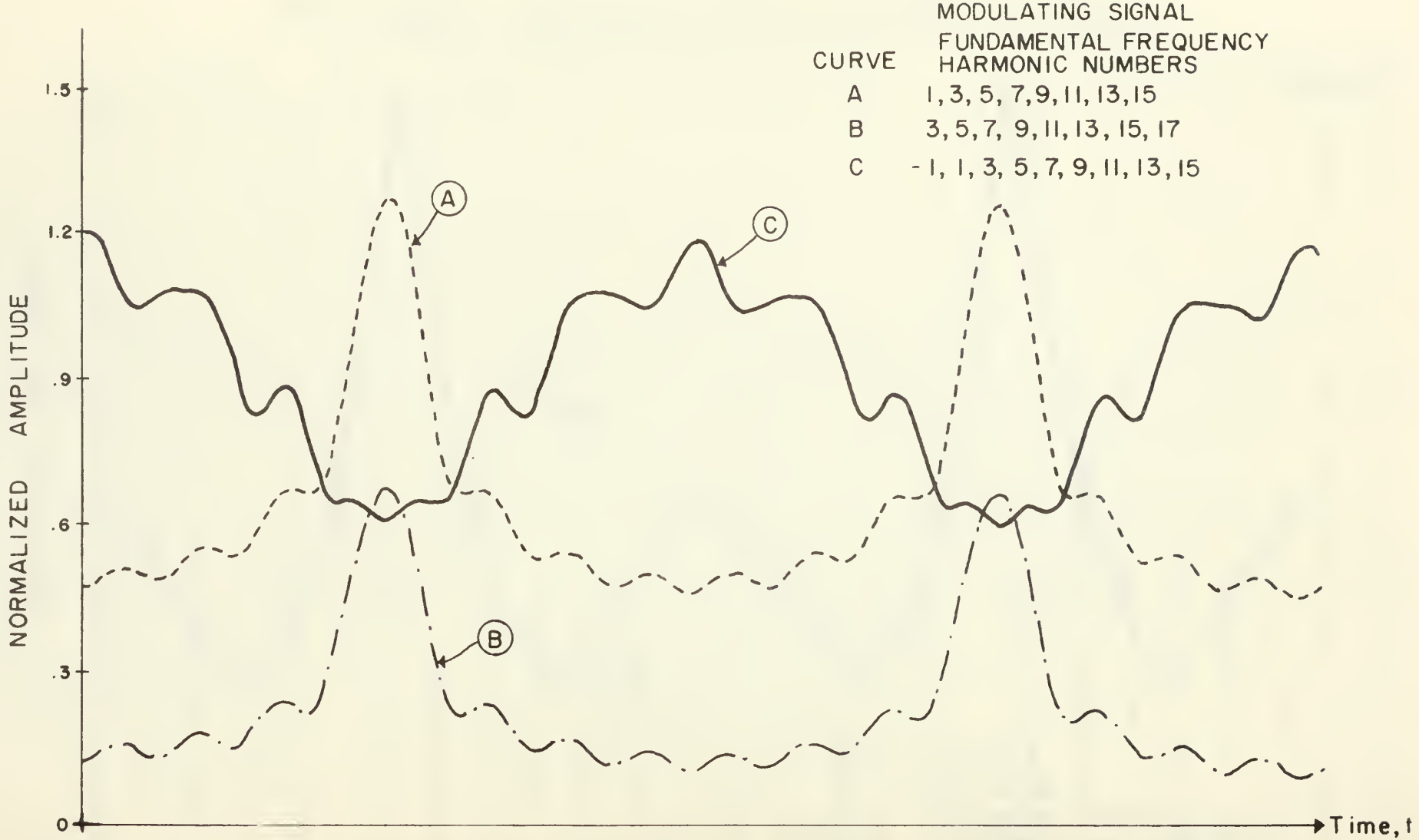

FIG. 18. EXAMPLES OF THE ENVELOPE OF THE OUTPUT OF THE PM-TO-AM CONVERTER (BANDPASS FILTER). Two sets of eight and one set of nine spectral components are considered.

the threshold detector as a pulse signifying a switch in the carrier

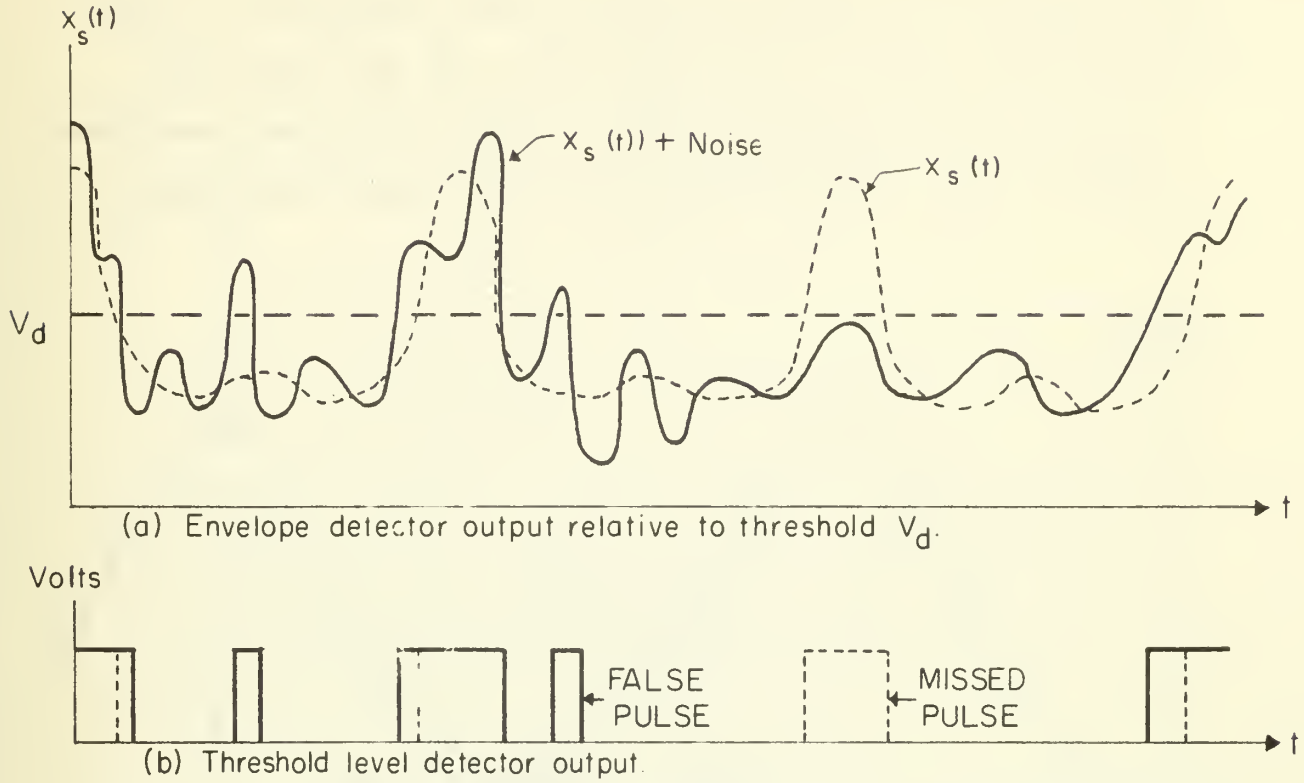

FIG. 19. WAVEFORMS ASSOCIATED WITH THE ASYNCHRONOUS DEMODULATION SYSTEM. The carrier is phase-reversal modulated by a square wave.

phase. When noise is present in the filter output, random fluctuations of the envelope occur. If these fluctuations cause the envelope to exceed V_d with no switch in carrier phase then a false pulse occurs in the threshold detector output. If the noise-generated envelope fluctuations depress the envelope below V_d, a pulse will be missing in the threshold detector output.

Calculation of the error statistics is not easily accomplished when the time waveform of the envelope is a continuously varying function. For the case of discrete (on-off) generation of the envelope the results are well known [Ref. 2, pp. 151-60; Ref. 9, pp. 159-70; Ref. 10, pp. 304-12; Ref. 11, pp. 287-95]. By dividing the switching interval into discrete periods of time and determining the time

average of the envelope of $v_f(t)$ in each period, the error probabilities may be approximated using the methods applicable to on-off keying of the carrier. With the aid of Fig. 20, the error probabilities can be determined for each interval. The system error probability is then obtained by averaging over the various intervals.

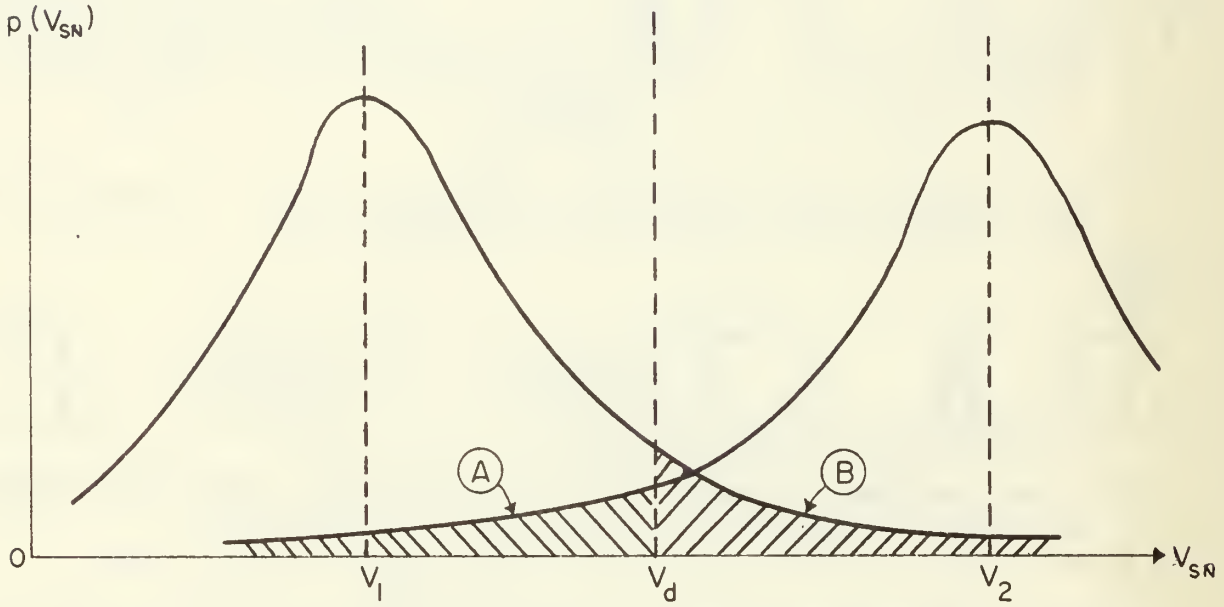

FIG. 20. CURVES OF THE PROBABILITY DENSITY FUNCTIONS OF ENVELOPE LEVELS WITH ADDITIVE GAUSSIAN NOISE. Shaded area A is the probability of a miss when the carrier envelope is at level V_1. Shaded area B is the probability of a false pulse occuring when the carrier envelope is at level V_2.

This calculation of the approximate probability of error for the asynchronous demodulation system is difficult, however, even for the case where the signal envelope $X_s(t)$ is expressed analytically (Eq. (13)). Such a calculation was not attempted in this study.

To reduce the error rate of the asynchronous demodulator, a pulse-width discriminator was considered. The PWD passes pulses from the level detector to the flip flop (see Fig. 22) only when the envelope

voltage $X_{sn}(t)$ exceeds a threshold level V_d for an interval of time in excess of a predetermined value T_d. The probability-of-error calculation in this case is equivalent to a solution of the zero-crossing problem. The zero-crossing problem (or in this case the level-crossing problem) is, in general, unsolved [Ref. 10, pp. 485-98; Ref. 12].

It was determined experimentally that minimum error rate for a given SNR was obtained when T_d was set approximately at one-fifth of the value of the interval during which the envelope $X_s(t)$ of $v_f(t)$ exceeds the threshold V_d. Somewhat surprisingly the threshold level V_d which minimized the error rate was approximately one-third the peak-to-valley difference voltage $\hat{X}_s$ above the minimum of the envelope.

Chapter 4

EXPERIMENTAL PROCEDURE

Two basic PRM detectors were considered in the experimental work: the coherent detection system shown in block diagram form as Fig. 21 and the asynchronous detection system shown in block diagram form as Fig. 22. Figs. 21 and 22 are partitioned to show the equipment and signals which would be associated with the transmitter, the propagation path and the receiver in a radio link. The transmitter equipment is common to both the coherent and the asynchronous detection systems considered.

A ring modulator is used to obtain the PRM signal. Fig. 23a shows the ring modulator circuit. The sinusoidal carrier is applied at port A and the modulating signal at port B. The resulting phase-reversal modulated carrier appears at port C. The operation of the ring modulator [Ref. 11, pp. 176-8] depends on the modulating signal E(t) applying bias to the switching diodes so that the paths which couple the input and the output are switched at each change of state of E(t). Figs. 23b, c, d and e show the operation of the modulator with the back-biased diodes omitted for clarity in each case. R_s is the modulating signal source impedance. Fig. 23 indicates that the output (port C) equals the input at port A or its inverse (180^o out of phase) depending on the state of the modulating signal E(t). Figs. 24a and b are typical photographs of the modulator output. A Relcom M1C double balanced mixer is used as the ring modulator.

The RF signal generator shown in Figs. 21 and 22 is a General Radio bridge oscillator Type 1330-A. The modulation source and clock-gate generators are Datapulse Model 101 pulse generators. The master

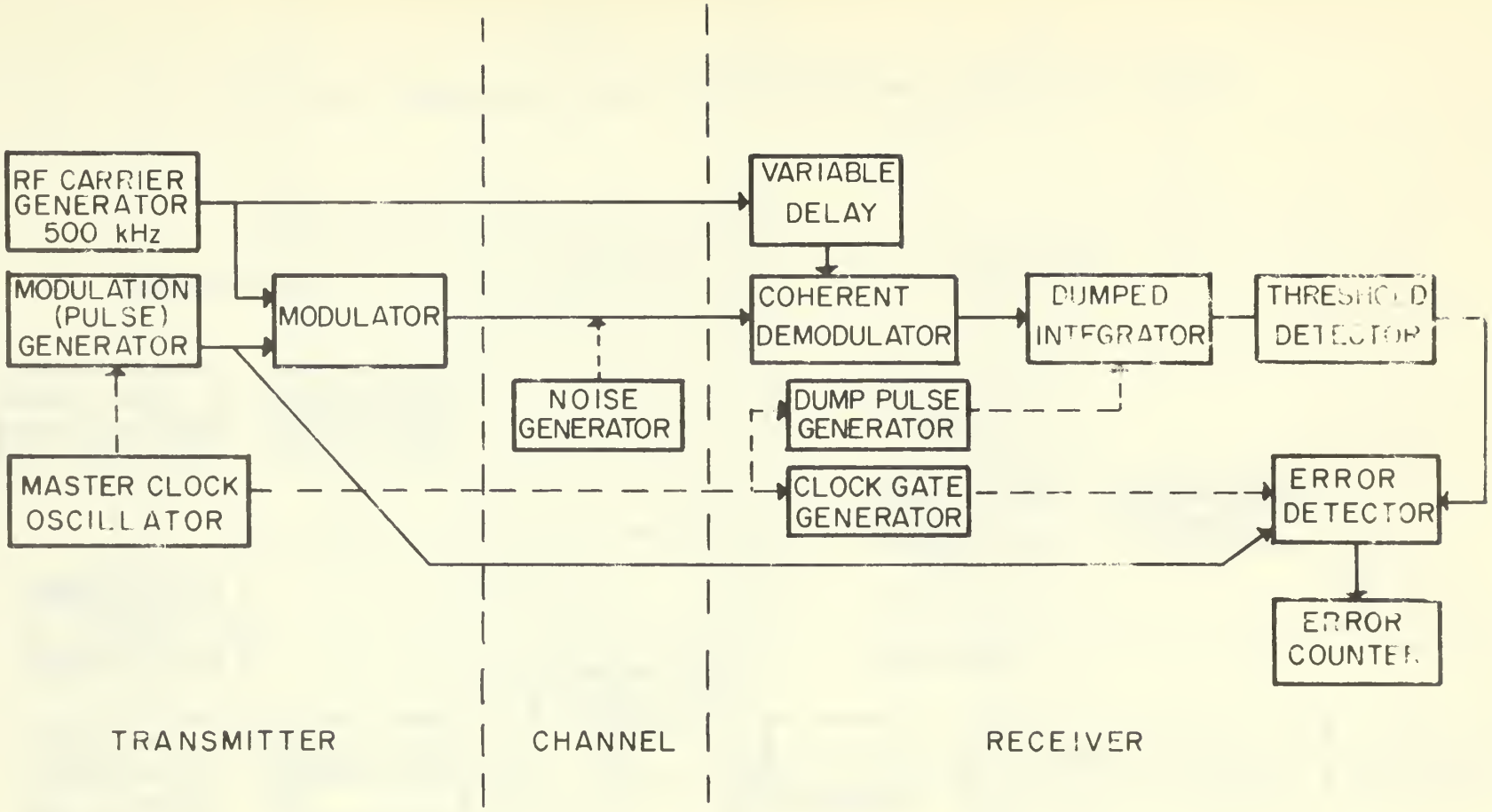

FIG. 21. BLOCK DIAGRAM OF THE EXPERIMENTAL COHERENT DEMODULATOR.

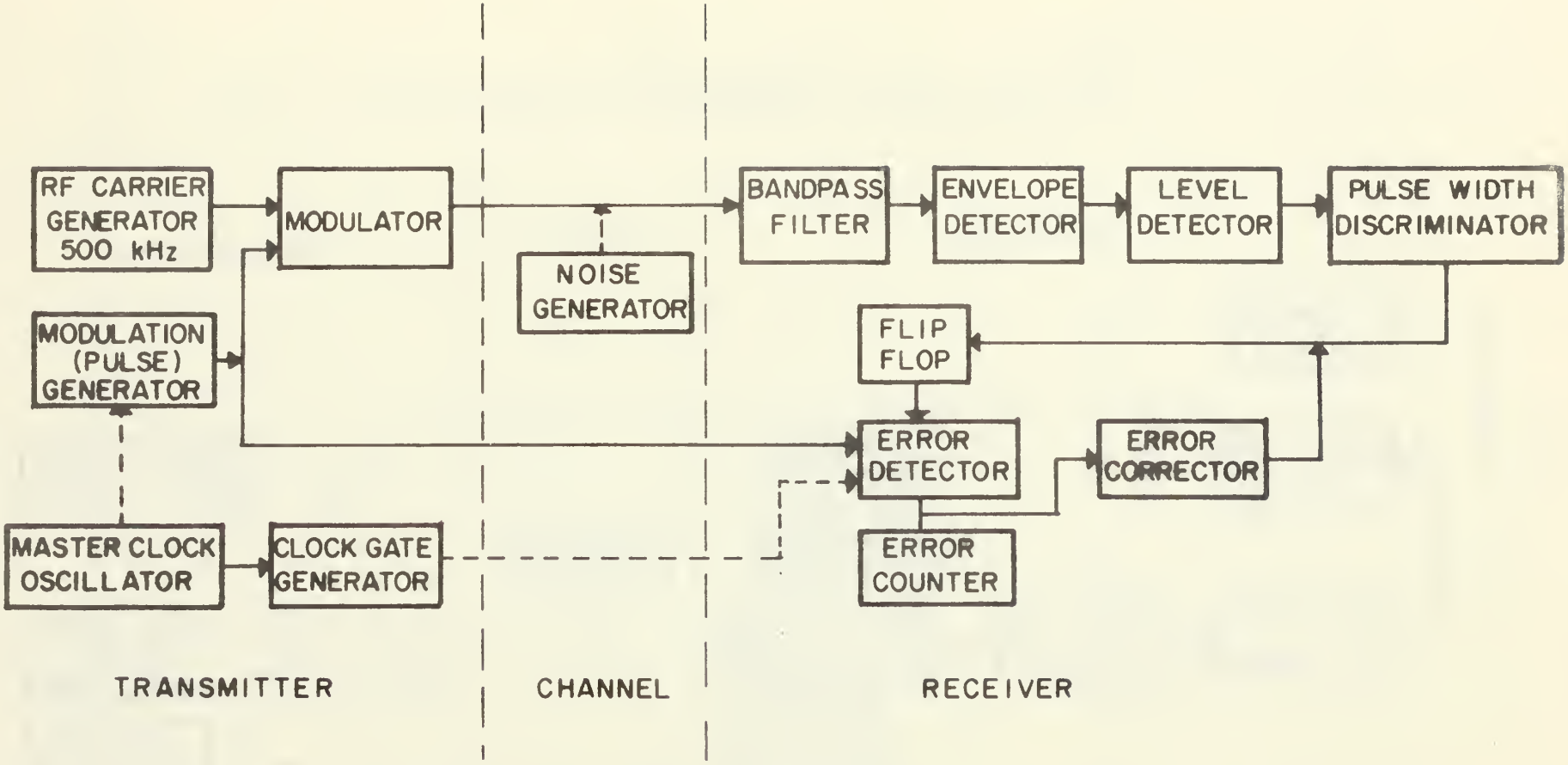

FIG. 22. BLOCK DIAGRAM OF THE EXPERIMENTAL ASYNCHRONOUS DEMODULATION SYSTEM.

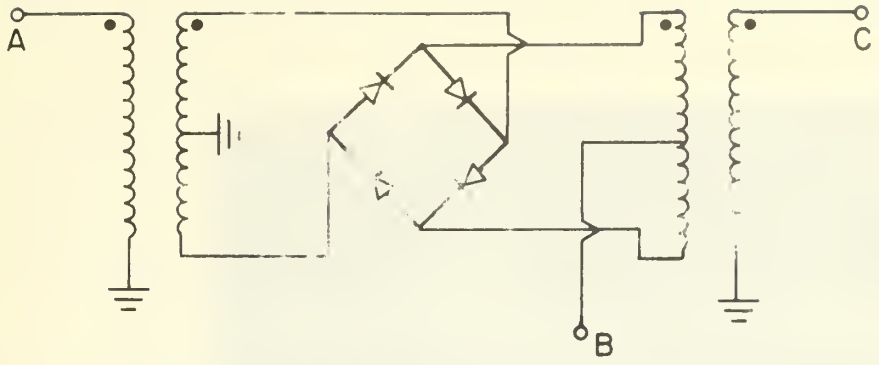

(a) Ring Modulator

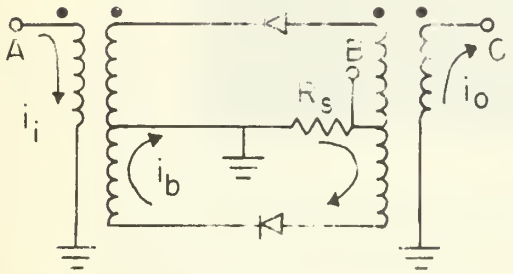

(b) E(t) is positive; port A has a positive potential.

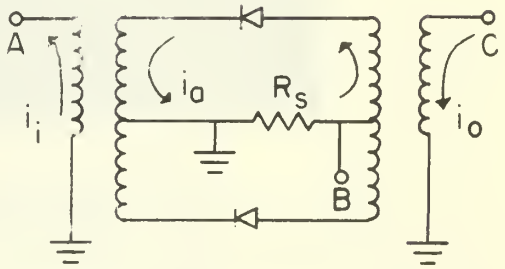

(c) E(t) is positive; port A has a negative potential.

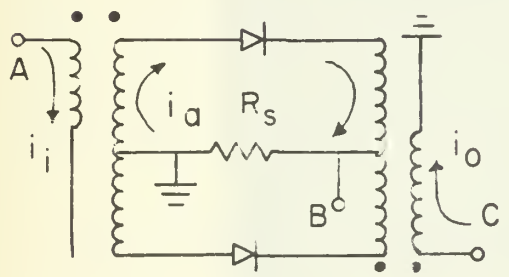

(d) E(t) is negative; port A has positive potential.

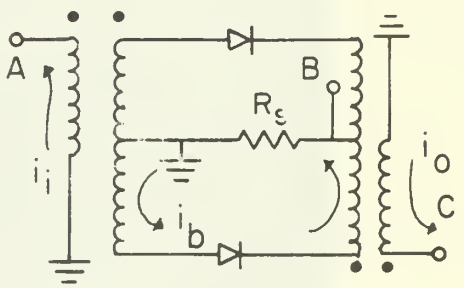

(e) E(t) is negative; port A has a negative; potential.

FIG. 23. CIRCUIT DIAGRAMS OF A RING MODULATOR AND OF EQUIVALENT AC CIRCUITS.

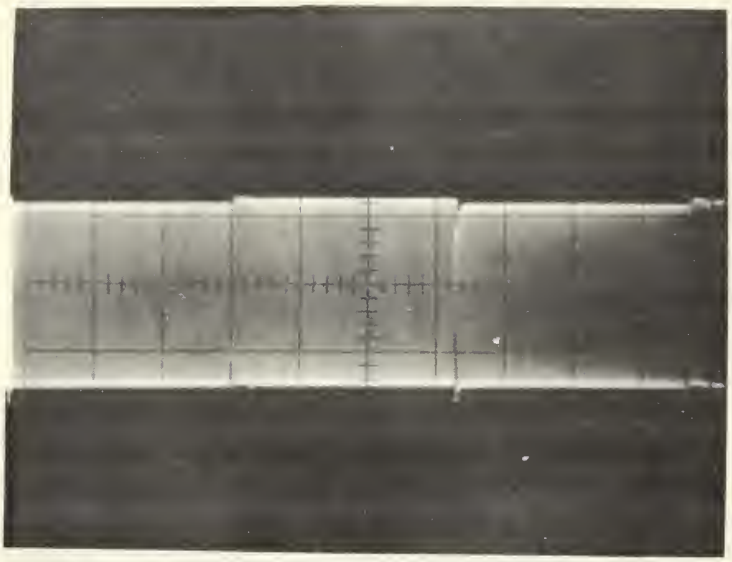

a. Compressed time scale.

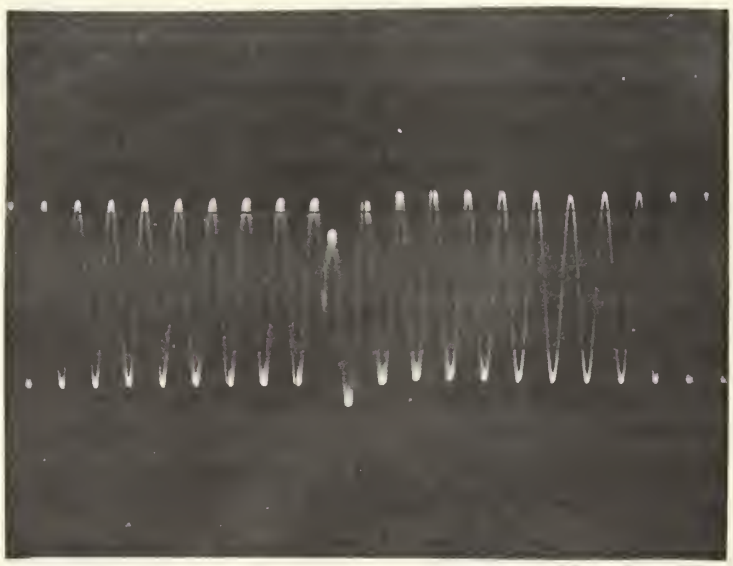

b. Expanded time scale.

FIG. 24. PHOTOGRAPHS OF THE OUTPUT OF A RING MODULATOR.

clock is a General Radio unit pulse generator Type 1217-B.

The rest of this chapter describes the individual elements of the two detection systems and details the techniques used to obtain the results.

A. Coherent Demodulation System

This section presents the components of the coherent demodulation system and then discusses the experimental procedure.

1. Circuitry

As shown in Fig. 21, the coherent demodulation system consists of a demodulator, integrator, threshold device and error counting circuitry.

a. Demodulator

A ring modulator identical to that used as the modulator is used as a demodulator. Its operation is slightly different, however. When the PRM signal is applied at port A of the circuit of Fig. 23a and a sinusoid of frequency f_o Hertz is applied at port C the ring modulator acts like a product device with the resulting product appearing at port B. The product s(t) of a PRM cosine wave v(t) and a reference cosine wave r(t) of the same frequency and phase is

$$s(t) = v(t)r(t) = [E(t)\cos\omega_o t][\cos\omega_o t] = E(t)[\tfrac{1}{2} + \tfrac{1}{2}\cos 2\omega_o t] \quad (14)$$

Since E(t) takes on values +1 or -1 only, then the DC term in Eq. (14) depends on the sign (phase) of E(t). Referring to Figs. 23b, c, d, and e the source resistance R_s becomes the load resistance developing the output voltage. The form of the AC term will not in practice be exactly as given by Eq. (14). The operating point on the characteristic curve of the diodes and hence the final form of the

output depends on the magnitudes of the signal and reference voltages. Fig. 25 shows a typical demodulator output waveform when the signal and reference voltages are approximately equal.

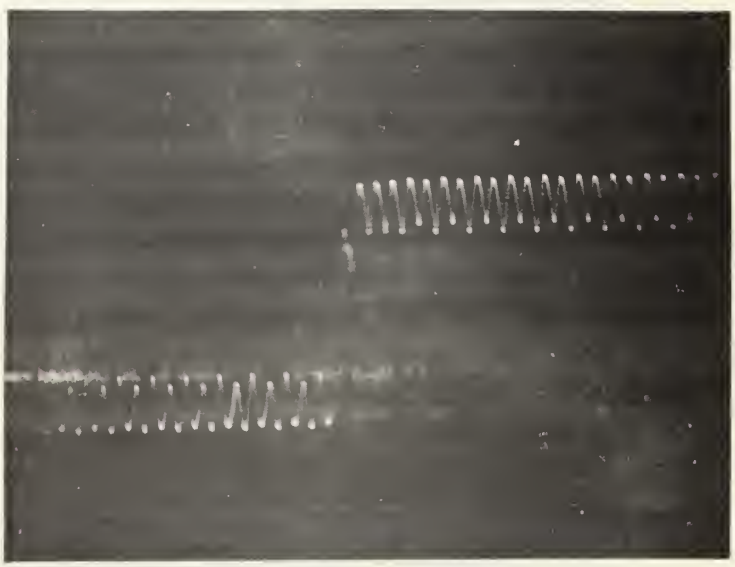

FIG. 25. PHOTOGRAPH OF THE OUTPUT OF THE COHERENT DEMODULATOR.

b. Integrator

In Fig. 21, the output of the coherent demodulator s(t) is integrated using a lowpass RC filter. The DC component of the demodulator output generates a positive or negative ramp function for E(t) positive or negative respectively. A signal of approximately 10 volts and one microsecond duration is generated by the master clock and used to dump the contents of the integrator at the end of each switching period by saturating a transistor shunting the capacitor in the RC filter. The dumped integrator output is amplified by a high input impedance amplifier to a peak level of approximately $\pm$1.5 volts and an adjustable DC level is applied to the ramp function before it excites the level detector.

c. Level Detector

The level detector in Fig. 21 is a Schmitt trigger circuit with adjustable trigger levels and is used to detect those levels of the ramp voltage representing the set threshold levels of the positive ramp (mark) and the negative ramp (space). In the absence of noise, the output of the Schmitt trigger is the restored modulation waveform E(t) delayed in time.

d. Error Detector

In Fig. 21 the error detector compares the level detector output (restored modulation waveform) with the original modulating waveform. A lack of coincidence in a switching interval is detected as an error. The clock gate compensates for the delay in the restored modulation waveform introduced by the integration and detection process. A Datapulse Model 101 pulse generator operating in the triggered variable-delay output mode is used for the clock-gate generator. The error detector output pulses are counted with a Hewlett-Packard FR 38/U frequency counter to obtain a cumulative error count. Details of the error detection circuitry are contained in Appendix B.

2. Test Procedure

Using the coherent demodulation system of Fig. 21, experimental data was compiled on the number of errors which occur in 20 successive ten-second periods at a data rate of approximately 6 kHz for various ratios of signal-to-noise power. This phase of the experiment also provides a basis for the measurement of signal-to-noise power ratios in a 1 MHz band by comparing these test results with the theoretical and experimental results of other authors [Ref. 5; Ref. 13]. Fig. 5 is a plot of the probability of error obtained in this study

vs. the signal-to-noise power ratio (SNR)

The noise generator of Fig. 21 is an Elgenco, Inc. Model 603A. The output of the noise generator in the 500 kHz band mode is mixed with a 500 kHz sinusoid to produce a 1 MHz band of Gaussian noise. The input and output amplitude spectra were observed to be of equal amplitude making it possible to use the noise spectral density conversion figures supplied with the noise generator directly. Additionally, the amplitude of the noise spectrum was compared with a monochromatic signal amplitude in the spectrum analyzer as a check on the conversion factors.

Signal power is determined by measuring the PRM carrier amplitude and calculating its RMS power. The energy per bit is found by dividing the signal power by the data rate [Ref. 3]. The ratio of E to N_o is then

$$E/N_o = 10 \log \frac{V_s^2/fm}{(V_n \times 1.2 \times 10^{-3})^2} \text{ db} \qquad (15)$$

where V_s is the RMS voltage of the PRM carrier, f_m is the data rate and V_n is the RMS voltmeter reading of the noise generator.

The effects of the addition of noise on the channel are seen in Figs. 26 and 27 which show the demodulator input and output respectively in an E/N_o environment of approximately one db. (Compare with Figs. 24a and 25.)

Figs. 28a and b respectively are photographs of typical integrator outputs when the channel is clear ($E/N_o \to \infty$) and when E/N_o is approximately 1 db.

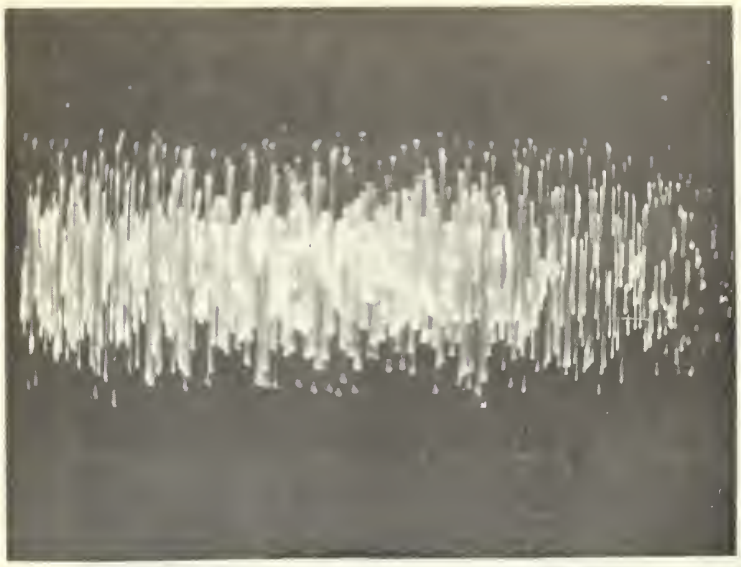

FIG. 26. PHOTOGRAPH OF THE SUM OF THE OUTPUT OF THE RING MODULATOR AND GAUSSIAN NOISE. The signal-to-noise ratio is 1 db.

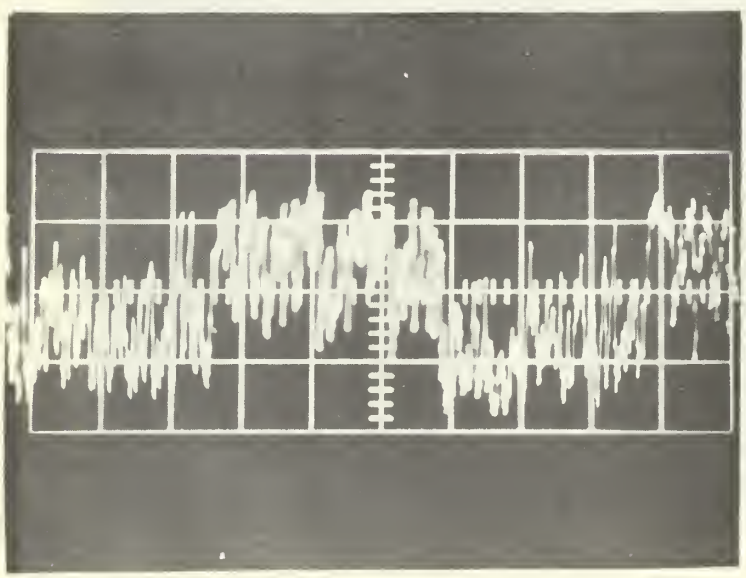

FIG. 27. PHOTOGRAPH OF THE OUTPUT OF THE COHERENT DEMODULATOR EXCITED BY THE MODULATED CARRIER PLUS GAUSSIAN NOISE. The signal-to-noise ratio is 1 db.

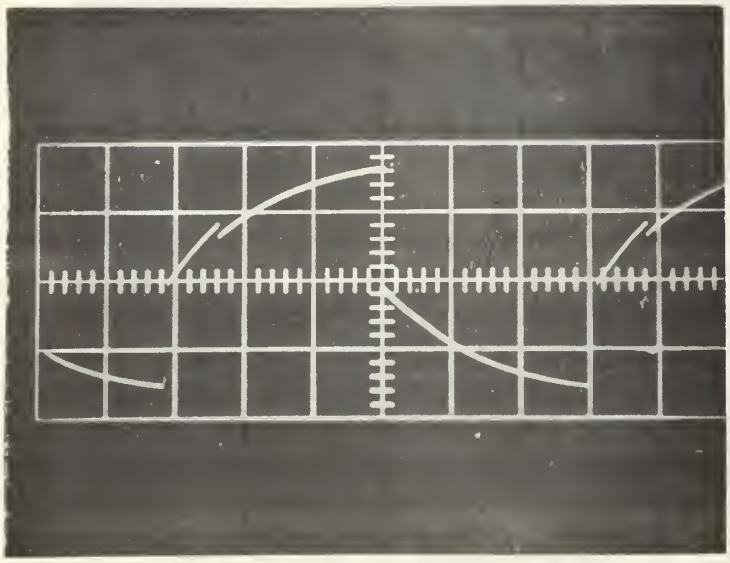

a. With carrier only.

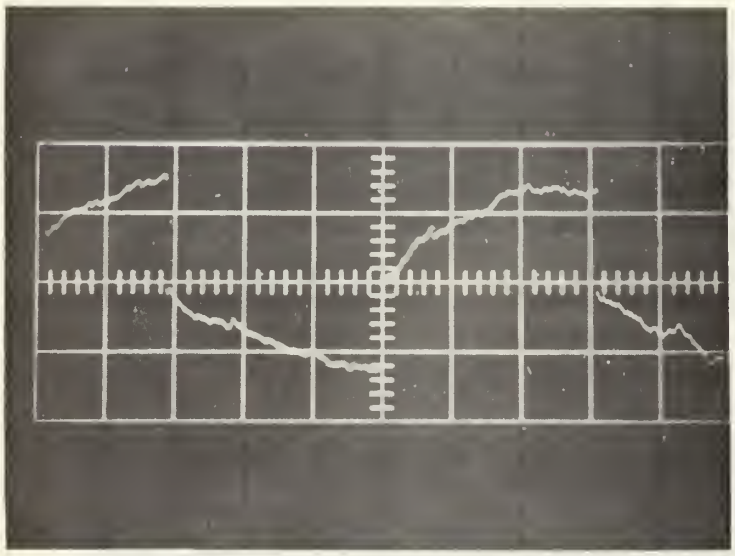

b. With carrier plus gaussian noise. The signal-to-noise ratio is 1 db.

FIG. 28. PHOTOGRAPHS OF THE OUTPUT OF THE INTEGRATOR OF THE COHERENT DEMODULATOR.

B. Asynchronous Demodulation System

This section presents the components of the asynchronous demodulation system and then discusses the experimental procedure.

1. Circuitry

As shown in Fig. 22, the asynchronous demodulation system considered in this study consists of a bandpass filter, envelope detector, threshold detector, pulse width descriminator, flip-flop circuit and error detector. Additional details on some of the circuits used in the asynchronous demodulation system are presented in Appendix B.

a. Mechanical Filter

As shown in Chapter 3 the asynchronous demodulation system first converts phase modulation to amplitude modulation and then detects the AM in a conventional manner. The PM-to-AM conversion is accomplished by filtering the PRM signal using a mechanical filter.

Preliminary investigation of the filter characteristics indicated a filter with band width sufficient to pass 6 to 10 side bands would be satisfactory. The relation between the minimum number of side bands (produced by square wave modulation) and the filter bandwidth is expressed by

$$B = (2n - 1)f_m \tag{16}$$

where B is the filter bandwidth in Hz, n is the number of side bands and f_m is the square-wave (modulation) frequency. Note that one cycle of the square wave modulation contains a mark and a space and therefore the data (switching) rate is $2f_m$. A filter bandwidth of 50 kHz, containing not less than 10 side bands, has a data rate of 5200 bits per second and for a minimum of 6 side bands a data rate of 9100 bits per second. These switching rates give reasonable latitude for

investigation of both higher and lower numbers of side bands. The Collins Radio Company F500-Y-500 mechanical filter was used in the experiment.

Measurements made of the attenuation vs. frequency characteristics of the filter actually used are presented in Fig. 29 together with the theoretical filter response (supplied by Collins Radio Co.). The lack of a "flat" filter response characteristic had to be compensated for by carefully choosing the sideband frequencies so that the input and output spectral components maintained as closely as possible the same amplitude relation. Additionally, it was not possible to find spectral components above five in number that would give a reasonable match from input to output.

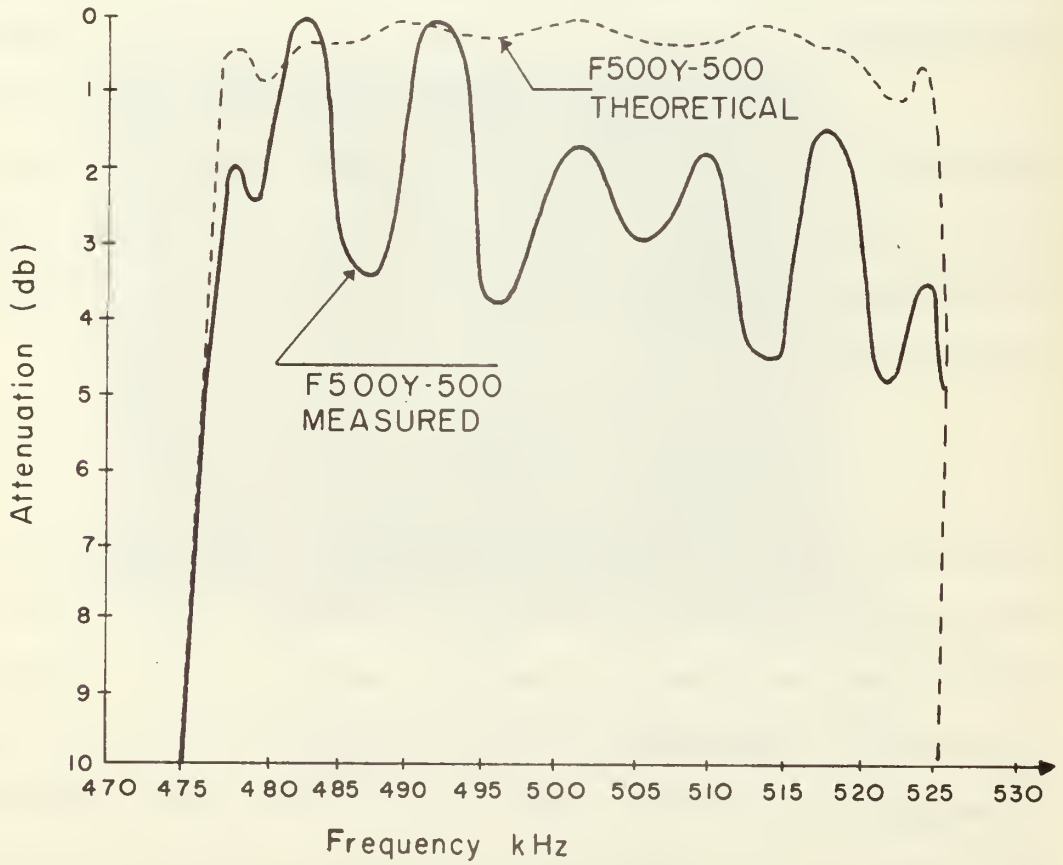

FIG. 29. PLOTS OF THE AMPLITUDE VS FREQUENCY RESPONSE OF THE MECHANICAL FILTER (PM-TO-AM CONVERTER).

Figs. 30a and b show respectively the input and output spectrum of the filter for four side frequencies.

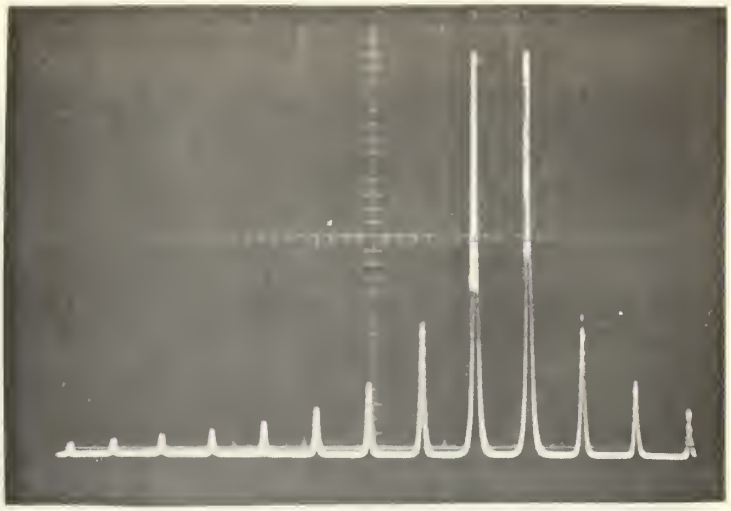

a. Unfiltered carrier (input to the filter).

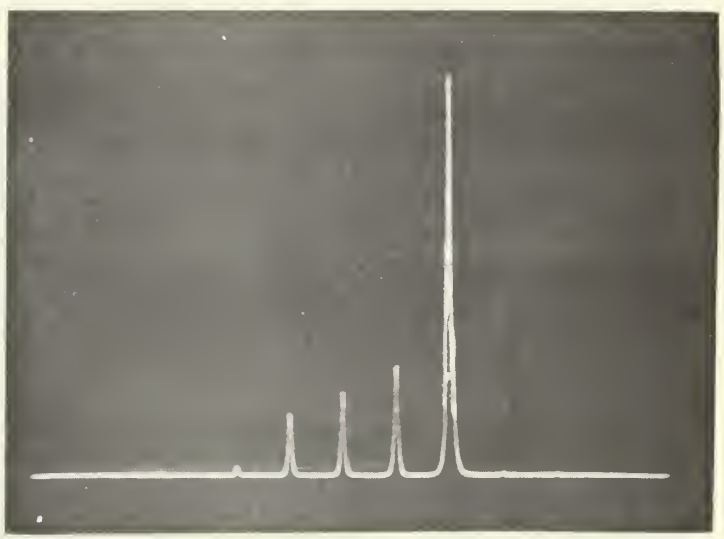

b. After filtering (output of the filter).

FIG. 30. PHOTOGRAPHS OF THE SPECTRUM OF A CARRIER PHASE-REVERSAL MODULATED BY A SQUARE WAVE. Four spectral components are retained by the filter.

Figs. 31a and b show respectively the input and output spectrum of the filter for six side bands and clearly illustrate the frequency characteristics of the mechanical filter used.

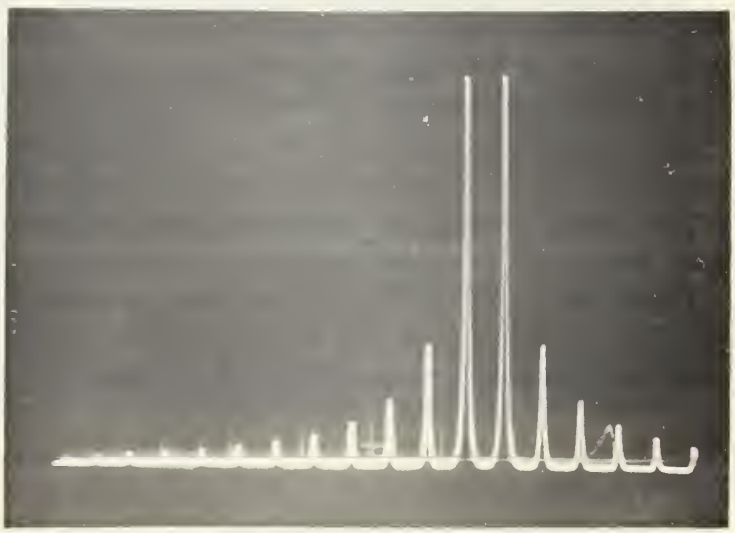

a. Unfiltered carrier (input to the filter).

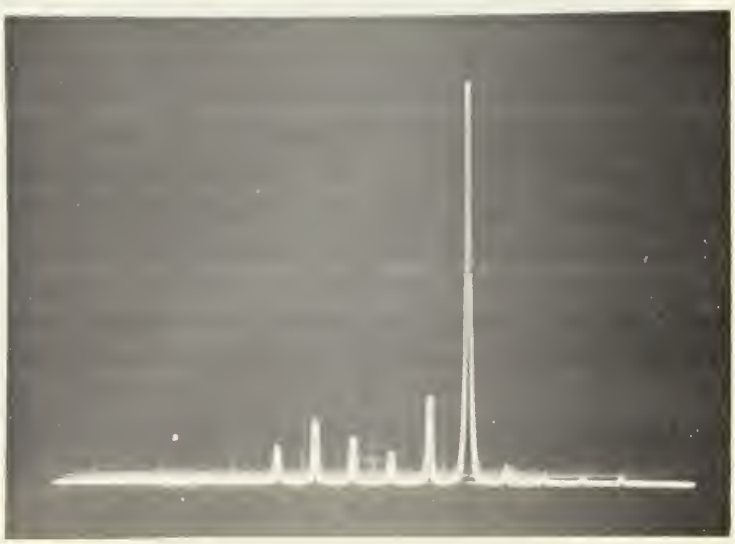

b. After filtering (output of the filter).

FIG. 31. PHOTOGRAPHS OF THE SPECTRUM OF A CARRIER PHASE-REVERSAL MODULATED BY A SQUARE WAVE. Six spectral components are retained by the filter.

b. Envelope Detector

The SSB filter of Fig. 22 is followed by an envelope detector. The filter converts the PRM signal to an AM signal having major lobes corresponding to the phase-reversals. The carrier is removed by the envelope detector. The envelope detector circuit is a half wave rectifier followed by a lowpass RC filter. It is noted that it is not necessary to accurately preserve the exact shape of the envelope and in fact this may not be possible with a fixed element circuit over a large range of switching rates. It was observed that slight attenuation of the higher order side frequencies did not affect the envelope peak-to-valley ratio, but this attenuation did reduce the side lobes. (See Figs. 32a and b.)

c. Threshold Detector

In Fig. 22, the envelope detector is followed by a Schmitt trigger which is realized with a single Fairchild RTμL 9914 (dual, two-input NOR gate) integrated circuit. The adjustable trigger levels are set to produce an output pulse whenever the major lobe of the carrier envelope occurs. The output of the Schmitt trigger is a pulse of 15-40 microseconds duration and of approximately 1.5 volts amplitude. The width of the pulse is a function of the wave shape of the envelope and of the trigger level.

d. Pulse Width Discriminator

The addition of noise at the input of the mechanical filter produces many large amplitude, short-duration pulses on the envelope of the carrier. These narrow pulses trigger the threshold detector. It was found that the error rate could be reduced (See Fig. 7) by using a pulse width discriminator (PWD) following the Schmitt trigger of Fig. 22. The PWD eliminates those pulses whose duration is

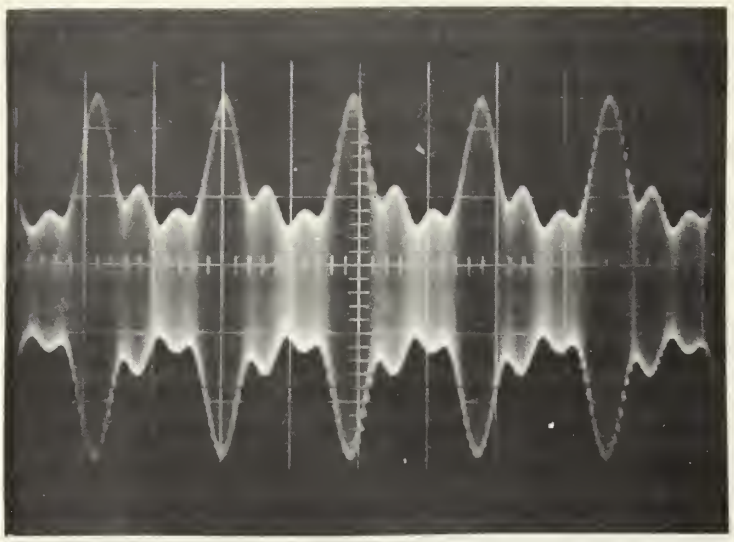

a. Output of the mechanical filter (PM-toAM converter).

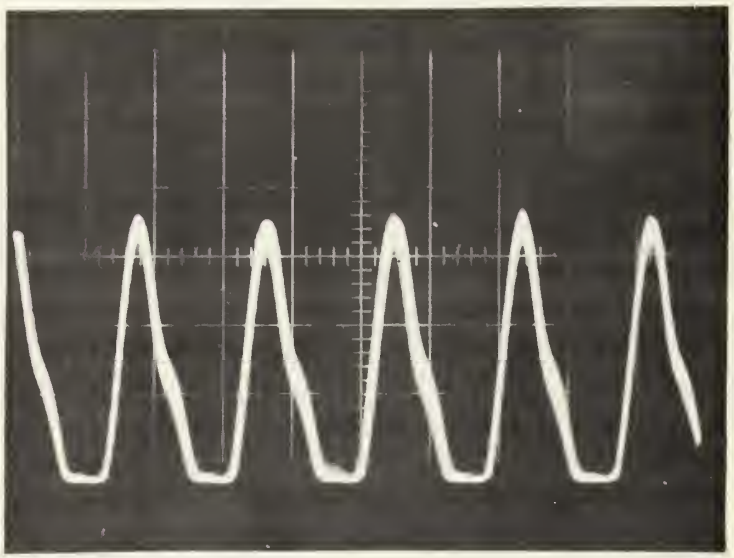

b. Output of the envelope detector. Note the suppression of the minor lobes of the envelope of the signal shown in (a).

FIG. 32. PHOTOGRAPHS OF THE CARRIER AND ENVELOPE RESULTING AFTER PM-TO-AM CONVERSION. The carrier is phase-reversal modulated by a square wave. Four spectral components of the modulated carrier are passed by the filter.

less than a preset (adjustable) value. The PWD circuit used in the experiment employs two Fairchild RTμL 9914 integrated circuits. The incoming pulse is delayed a set length of time T_d and this delayed replica of the pulse is used as a gating signal. The undelayed pulse will cause a positive pulse in the output of the PWD coincidence gate only when the delayed replica pulse also exists. Thus if the incoming pulse duration is shorter than the delay there is no output from the PWD. The details of the circuit and operation of the PWD are presented in Appendix B.

e. Flip Flop

The input to the flip flop of Fig. 22 is a positive pulse corresponding in time to a major lobe of the envelope (180^o phase switch) if the pulse is of sufficient duration to be passed by the pulse width discriminator. This positive pulse is inverted twice and amplified to 3.6 volts. The additional inversion will be explained in the following section.

The 3.6 volts positive pulse is applied at the CP terminal of a Fairchild RTμL 9923 (JK Flip Flop). The other input terminals of the flip flop are grounded and the resultant output is a pulse train where each pulse is switched on by the positive going edge of the input pulse and switched off by the positive-going edge of the next pulse. Thus the output of the flip flop corresponds to the modulation input wave form or its inverse delayed in time.

f. Error Detector

The error detector used in the asynchronous detection system of Fig. 22 is identical to that of the coherent detection system of Fig. 21. This method of restoring the modulation is ambiguous in the sense that it is not known whether the modulating signal or its inverse

is present at the output of the flip flop. If the inverse is present, which would occur in the event of a missed pulse or a false pulse, the error detector records an error for each successive bit until the reference and detected waveforms are returned to coincidence. These additional error counts are not actual errors in the differential detection system and must be eliminated from the error count. This is accomplished by feeding back a narrow pulse from the output of the error detector to "correct" the previous error. The output of the error detector is differentiated to obtain a narrow (approximately three microsecond) positive pulse. This pulse is amplified, delayed by about four microseconds and reinserted at one input of a NOR gate (the output of the pulse width discriminator being the second input to this NOR gate). The NOR gate output is inverted and applied to the flip flop. This additionally inserted pulse causes a change of state at the output of the flip flop bringing the detected pulse in coincidence with the reference.

2. Test Procedure

In Fig. 22 the error detector supplies negative pulses to the error counter. A Hewlett-Packard FR-38/U frequency counter with video amplifier unit is used to count errors in 20 successive 10 second intervals. These errors are basically single switching errors but several errors may be produced in one clock gate interval.

The noise generator (Elgenco, Inc. Model 603A) output is applied to the filter input. The voltage in the 50 kHz band at the filter output is measured with a AN/USM - 106 voltmeter. The AN/USM - 106 voltmeter is a broad band AC voltmeter which accurately reads the RMS voltage of a monochromatic wave. This voltmeter also reads a voltage proportional to the RMS value of a complex signal containing

two or more frequency components. The ratio of the voltage reading V_s of the signal alone (containing several side frequencies) to the voltage reading V_n of the noise alone is a measure of signal to noise ratio in a 50 kHz band:

$$S/N = 20 \log_{10} V_s/V_n \qquad (17)$$

This relation is verified by comparison with the amplitude spectra observed using a spectrum analyzer.

In the experiment, data rates of 8 kHz to 12 kHz were used (single switching periods of 80 to 120 microseconds). The time delay in the detected waveform was typically 25% of the switching interval. As the number of side bands increases, the major peaks of the envelope increase in amplitude and become narrower; however, the delay is additionally a function of the trigger level, transmission delays and time jitter introduced by noise, etc. The 25% delay results in approximately 50% of the switching interval when the detected and reference wave form coincide. The coincidence interval is further reduced by early or late triggering caused by noise, etc. The result is that a maximum clock-gate width of 30% of the switching period is optimum in the sense that false errors are not generated and an excessive number of true errors are not omitted from the count.

Experimental trials using different clock-gate widths show that the probability of error for a given signal-to-noise ratio is a weak function of the clock-gate width. As shown in Fig. 33, the clock-gate width does not change the basic shape of the P_e vs. SNR curve in the range of practical interest [P_e less than 10^{-2}], but it does shift the curve by about one db to the right when the clock gate is increased from 5 to 30 microseconds while holding all other parameters

constant. It was necessary to pick some standard clock-gate width for the remaining experiments. Considering the data rates necessary to limit the side band content of the filtered signal it was decided to use a standard clock gate of 15 microseconds duration.

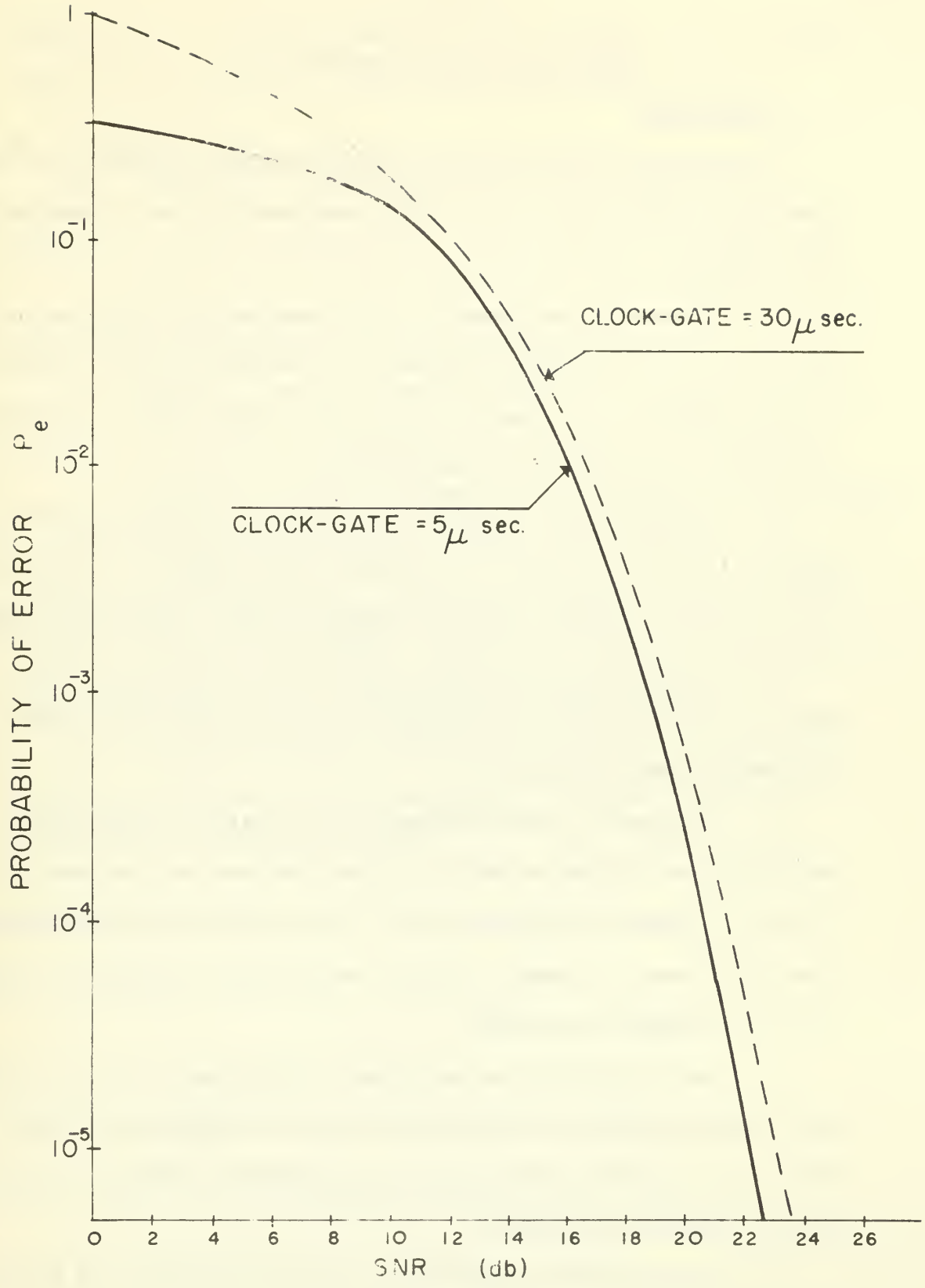

FIG. 33. EXPERIMENTALLY DERIVED CURVES SHOWING THE EFFECT OF THE CLOCK-GATE WIDTH ON THE ERROR COUNT.

Chapter 5

CONCLUSIONS AND RECOMMENDATIONS

A. Conclusions

A number of conclusions concerning asynchronous demodulation of a phase-reversal-modulated carrier have been drawn and are presented in this chapter.

1. The measured performance of the asynchronous demodulation system relative to the optimum performance of coherent systems requires an approximately 12 db larger signal-to-noise power ratio for the same probability of error [Ref. 2, pp. 225-39].

2. The asynchronous demodulation system is relatively easy to design and may use circuits and components that require a minimum of sophistication in construction and operation. The asynchronous demodulation system used in this report consists of a bandpass filter, a conventional AM detector and two basic logic circuits (pulse width discriminator and flip flop).

3. A modulation system designed for use with an asynchronous demodulator may be simpler and less expensive than one designed for use with a coherent demodulator. This is so because an asynchronous demodulator does not demand a highly stable carrier frequency or data rate for successful operation.

4. A given asynchronous demodulator design may be used to monitor various data channels having different carrier frequencies or data rates. Such diverse applications are not generally possible with many coherent demodulator designs.

5. The asynchronous demodulation system performance may be improved by lowering the data rate (passing a greater number of spectral components through the fixed bandpass filter) without requiring a readjustment of the receiver. This can be contrasted with the bandlimited

differentially coherent demodulator, which requires that the delay line in the receiver be changed when the data rate is changed.

B. Recommendations

The investigation conducted in this study suggests several additional areas of investigation. Some of these are listed here.

1. Extend work to consider other means of reducing effects of noise on the asynchronous demodulation system.

2. Improve the error detection process to permit an exact comparison of the demodulated waveform and modulating waveform E(t).

3. Investigate system performance using random modulating signals.

4. Conduct a computer simulation of the statistical properties of the asynchronous demodulation system with the pulse width discriminator (and any future improvements) to determine the optimum values of various system parameters under a variety of operating conditions.

5. Study the effect on system performance of using different filtering techniques including weighting of spectral components.

REFERENCES

1. D.F. Hoth, "Digital Communications," Bell Laboratories Record, pp. 38-43; Feb. 1967.

2. W.R. Bennett and J.R. Davey, Data Transmission, McGraw-Hill Book Co., New York, N.Y.; 1965.

3. J.G. Lawton, "Comparison of Binary Data Transmission Systems," Proceedings of the 2nd National Convention of Military Electronics, pp. 54-61; Jun 1958.

4. J.G. Lawton, "Theoretical Error Rates of 'Differentially Coherent' and 'Kineplex' Data Transmission Systems," Proc. IRE, pp. 333-4; Feb 1959.

5. C.R. Cahn, "Performance of Digital Phase Modulated Communications Systems," IRE Trans. on Communication Systems, pp. 3-6; May 1959.

6. A. Viterbi, "Optimum Detection and Signal Selection for Partially Coherent Binary Communications," IEEE Trans. on Information Theory, pp. 239-46; Apr 1965.

7. M. Schwartz, Information Transmission, Modulation and Noise, McGraw-Hill Book Co., New York, N.Y.; 1959.

8. R.C. Cumming, Personal correspondence and notes, Stanford Univ., Stanford, California; Mar 1966.

9. P.F. Panter, Modulation, Noise and Spectral Analysis, McGraw-Hill Book Co., New York, N.Y.; 1965.

10. A. Papoulis, Probability, Random Variables and Stochastic Processes, McGraw-Hill Book Co., New York, N.Y.; 1965.

11. M. Schwartz, W.R. Bennett and S. Stein, Communications Systems and Techniques, McGraw-Hill Book Co., New York, N.Y.; 1966.

12. G.A. Myers, "A Commentary on the Zero Crossing Problem with a Note on the Multivariate Gaussian Distribution," T.R. No. 2014-1, Stanford Univ., Stanford, Calif.; Jun 1964.

13. A.B. Glenn, "Comparison of PSK vs FSK and PSK-AM vs FSK-AM Binary Coded Transmission Systems," IRE Trans. on Communications Systems, pp. 87-100; Jun 1960.

14. Y. Chu, Digital Computer Design Fundamentals, McGraw-Hill Book Co., New York, N.Y., pp. 110-8 and 128-30; 1962.

Appendix A

DIFFERENTIATION AS AN ASYNCHRONOUS METHOD OF DETECTION OF A PHASE-REVERSAL MODULATED CARRIER

As shown in Chapter 3, the expression for a phase-reversal-modulated carrier is

$$v(t) = E(t)\cos\omega_o t \tag{2}$$

where E(t) is the modulating function having values +1 or -1. If this wave form is differentiated the resulting expression is

$$v'(t) = E'(t)\cos\omega_o t - \omega_o E(t)\sin\omega_o t \tag{A-1}$$

where the prime denotes differentiation. Eq. (A-1) shows the differentiated output represented as the sum of inphase and quadrature carrier terms. The quadrature term has the same form as the modulated carrier. The term E'(t) is a train of alternately positive and negative spikes (approximately delta functions). The disadvantage of this method of demodulation is immediately apparent by an examination of the first term of Eq. (A-1). The bipolar spikes are modified by the term $\cos\omega_o t$ and thus the spike amplitude and polarity will depend on the value of $\cos\omega_o t$ at the time of switching of E(t). In an asynchronous system there is no fixed relation between the modulation and the carrier phase. Therefore, although some spikes will appear at full amplitude, some will be diminished and some will be eliminated; i.e., those nonzero values of E'(t) which occur when t is such that $\omega_o t = k\,\pi/2$ for k an integer. Fig. A-1 is a single trace photograph of the output of a differentiator (high pass CR filter) which shows the variation in spike amplitude. Due to the narrowness of the spikes this photo was retouched to show the spikes clearly.

A second consideration which makes this method generally unacceptable is apparent from Fig. A-2 which shows the same signal and added Gaussian noise (SNR = 12 db) at the differentiator output. The noise voltage level and form after differentiation makes threshold detection of E'(t) difficult even at moderate signal-to-noise power ratios. For these reasons, investigation of the use of a differentiator as an asynchronous demodulator was not considered further.

FIG. A-1. PHOTOGRAPH OF THE OUTPUT OF A DIFFERENTIATOR EXCITED BY A CARRIER WHICH HAS BEEN PHASE-REVERSAL MODULATED BY A SQUARE WAVE. Note the variable amplitudes of the voltage spikes which occur at the phase reversals of the carrier.

FIG. A-2. PHOTOGRAPH OF THE OUTPUT OF A DIFFERENTIATOR EXCITED BY THE SUM OF A CARRIER WHICH HAS BEEN PHASE-REVERSAL MODULATED BY A SQUARE WAVE AND GAUSSIAN NOISE. The signal-to-noise ratio is 12 db.

Appendix B

DETAILS OF CIRCUITS USED IN THE ASYNCHRONOUS DEMODULATION SYSTEM

This appendix details some of the circuits used in the experiment. The envelope detector and Schmitt trigger are typical of those found in standard reference works and are employed in the same manner. Therefore, these circuits are presented without comment. Figs. 21 and 22 and the text of Chapter 4 indicate the complete network containing these circuits.

Fig. B-1 shows the circuit of the envelope detector. Envelope detection is accomplished by the diode and the two stage RC low pass filter as shown. The envelope is amplified and clamped to ground potential.

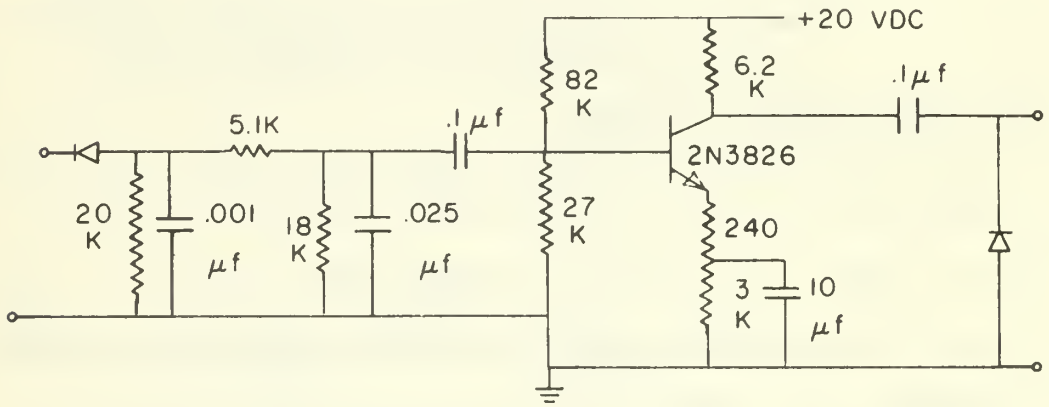

FIG. B-1. CIRCUIT DIAGRAM OF THE ENVELOPE DETECTOR.

Fig. B-2 shows the Schmitt trigger circuit used as the level detector. The circuit consists of one Fairchild RTμL 9914 (dual, two-input NOR gate) integrated circuit and two potentiometers. The 500 ohm potentiometer controls the trigger level and the 6000 ohm potentiometer

controls the retrigger (reset) level and the output pulse amplitude.

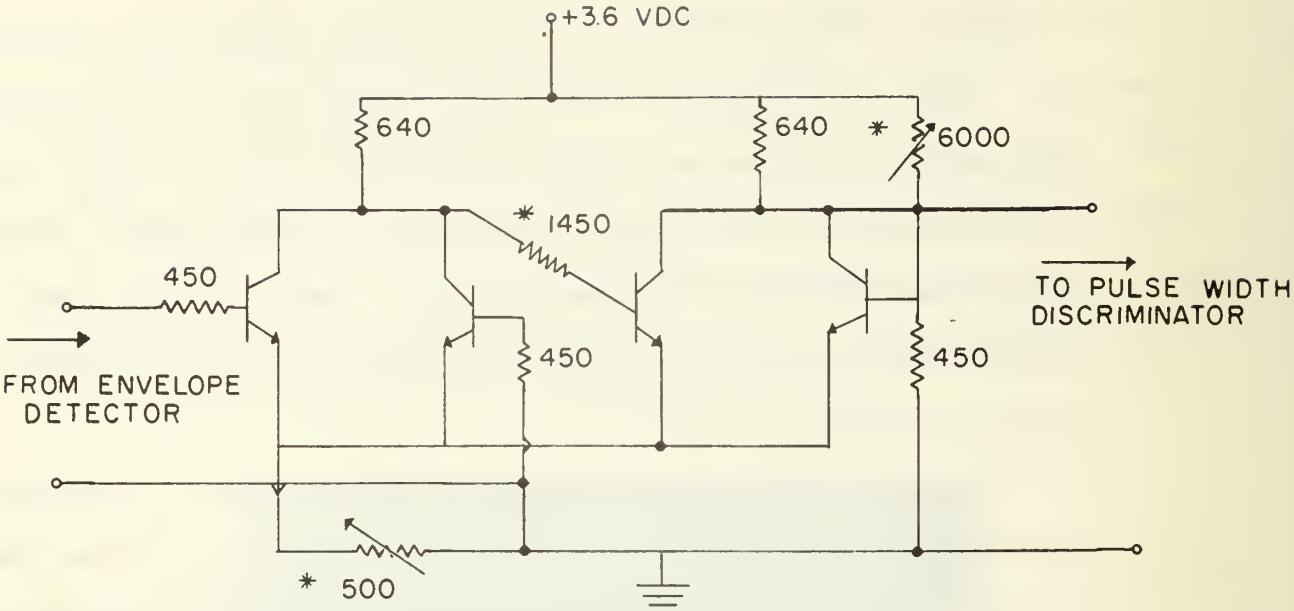

FIG. B-2. CIRCUIT DIAGRAM OF THE SCHMITT TRIGGER. Components labeled with an asterisk are external to the Fairchild RTμL 9914 integrated circuit.

A. Pulse Width Discriminator

The pulse width discriminator shown in Fig. B-3 utilizes two

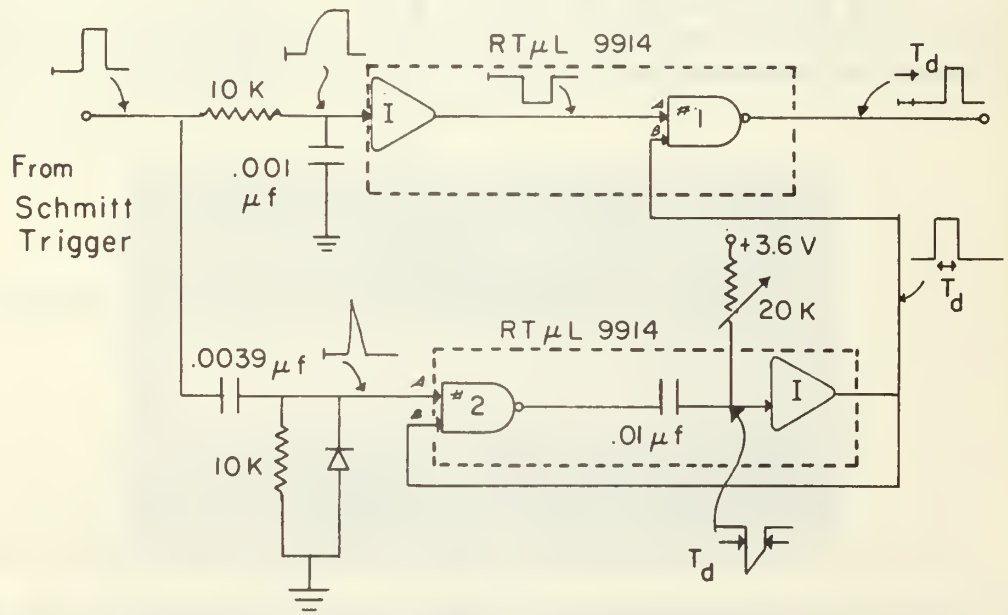

FIG. B-3. SCHEMATIC DIAGRAM OF THE PULSE WIDTH DISCRIMINATOR.

Fairchild RTμL 9914 integrated circuits. A positive pulse of about 1.5 volts is produced at the input of the discriminator when the Schmitt trigger is activated. The RC low pass filter in the upper branch causes the voltage to rise slowly to approximately 0.9 volts before the output of the inverter responds with a drop from 3.6 to 0 volts. The voltage at input A of NOR Gate #1 is a slightly delayed negative pulse of approximately the same duration as that of the Schmitt trigger input pulse. The RC time constant of the filter determines the delay and also the minimum-width pulse that the discriminator will pass. In the lower branch the high-pass filter and clipper produces a fast rise time pulse which decays slowly until the Schmitt trigger pulse turns off. The resulting negative pulse at the output of NOR Gate #2 is transmitted by the .01 uf capacitor to the inverter and causes a positive pulse to appear at the B input of NOR Gates #1 and #2. This pulse will persist until the .01 uf capacitor can recharge to a voltage sufficient to switch off the inverter and terminate the pulse. At NOR Gate #2 the inverter pulse (B input) insures the NOR Gate output will not go positive until the capacitor is recharged to the inverter cut off level. At NOR Gate #1 the B input positive pulse blocks any output (A is zero, B is positive and output is zero) until B input returns to zero. If the A input negative pulse persists after the B input pulse is removed, a positive output pulse results. If the A input pulse turns off early, the pulse at inputs A and B of NOR Gate #1 terminates with no output from the discriminator occurring.

B. Error Detector

The error detector must determine when the original modulating wave form and the restored form of the modulation are not in exact

agreement. To accomplish this an "exclusive OR" logic circuit was utilized followed by a timing-gate circuit. [Ref. 14] The circuit in Fig. B-4 employs three Fairchild RTμL 9914 and one RTμL 9900 integrated

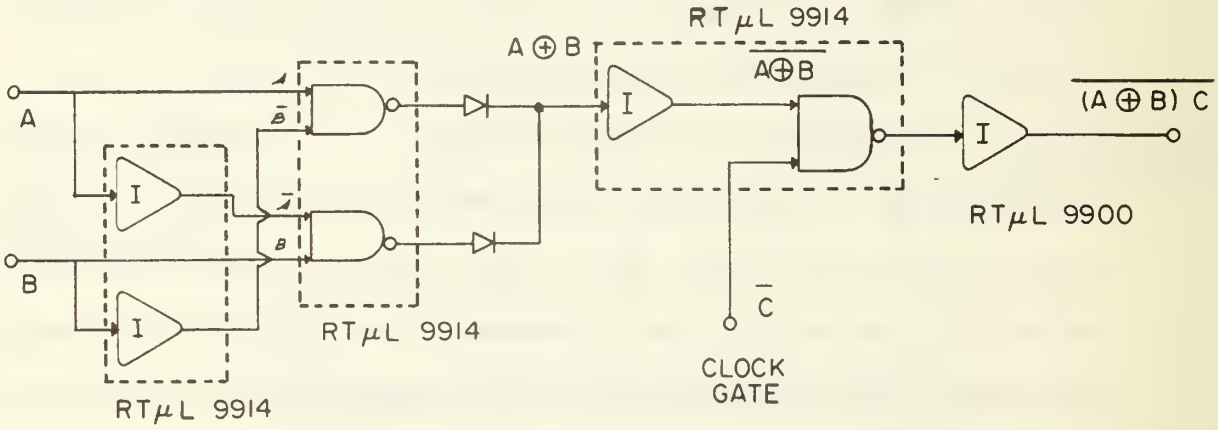

FIG. B-4. SCHEMATIC DIAGRAM OF THE ERROR DETECTOR.

circuits. The error detector compares the reference signal (A) and the detected signal (B) and will give a positive pulse out when A and $\overline{B}$ are both zero or when B and $\overline{A}$ are both zero, thereby forming $A \oplus B$ logic ($A \oplus B = \overline{A} \cdot B + A \cdot \overline{B} = \overline{A \odot B}$).

The A + B is then inverted to produce the coincidence function $A \odot B = \overline{A}\,\overline{B} + AB = \overline{A \oplus B}$. The clock-gate pulse applied to the next NOR gate is negative and is represented by $\overline{C}$. The logical expression is $\overline{(A \oplus B)} + \overline{C} = (A \oplus B) \cdot C$ which is inverted by the RTμL 9900 to form $\overline{(A \oplus B) \cdot C}$. Thus if A and B are not in exact coincidence during the clock gate interval, a negative pulse appears at the output of the error detector.

C. Error Correction Loop

The necessity for and the operation of the error correction loop is illustrated in Chapter 4. Fig. B-5 shows the complete loop. When an

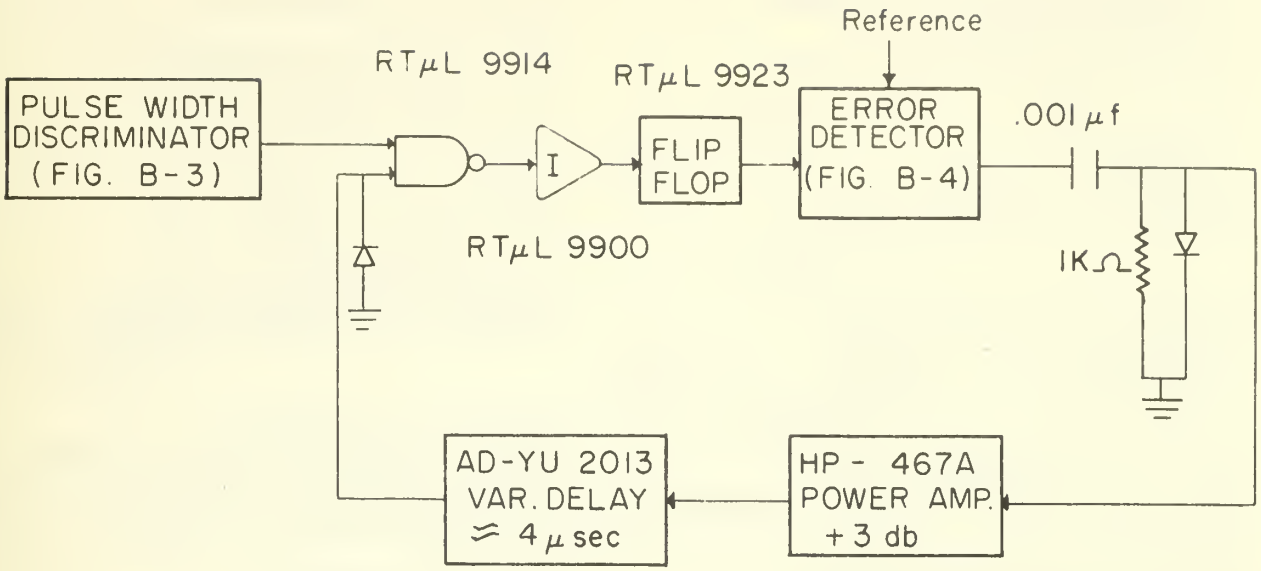

FIG. B-5. BLOCK DIAGRAM OF THE ERROR CORRECTION SYSTEM.

error is detected the RC high pass filter differentiates the error pulse producing first a negative and then a positive voltage spike of about 3μsec duration. The diode clips off the positive pulse. The negative pulse is amplified by a Hewlett-Packard 467A power amplifier and delayed and inverted by an AD-YU 2013 lumped constant variable delay line. The resulting positive pulse is clamped to ground potential and applied to one input of a dual NOR logic circuit (one half of a Fairchild RTμL 9914). This NOR gate accepts positive pulses from the pulse width descriminator or from the correction loop. Either pulse will cause a change of state of the flip flop, thus correcting the detected error. The exact delay in the correction loop is a function of the pulse width out of the PWD and is set to insure that the longest of these pulses has passed before the error-correction pulse arrives.

DISTRIBUTION LIST

Defense Documentation Center
Cameron Station
Alexandria, Virginia
Attn: IRS (20 copies)

Library
Naval Postgraduate School
Monterey, California 93940
(2 copies)

Naval Security Group Hdq.
3801 Nebraska Ave., N.W.
Washington, D. C. 20390
Attn: G-43 (3 copies)

Naval Ship Systems Command
Navy Department
Washington, D. C. 20360
Attn: W. Steed, Code 6050C

Commanding Officer and Director
Naval Electronics Laboratory Center
San Diego, California 92152

Commander
Naval Electronics Systems Command
Navy Department
Washington, D. C. 20360

Director Naval Research Laboratory
Washington, D. C. 20390

Office of Naval Research
Navy Department
Washington, D. C. 20305
Attn: Code 427

Librarian
Systems Techniques Laboratory
Stanford University
Stanford, California 94305

CDR F. A. Rudolph, Jr.
c/o Commander
Charleston Naval Shipyard
U. S. Naval Base
Charleston, South Carolina

Prof. Glen A. Myers
Department of Electrical
Engineering
Naval Postgraduate School
Monterey, California 93940
(3 copies)

Prof. C. E. Menneken
Dean of Research Administration
Naval Postgraduate School
Monterey, California 93940

Dr. R. C. Cumming
Applied Electronics Laboratory
Stanford University
Stanford, California 94305

DOCUMENT CONTROL DATA - R & D

Security classification of title, body of abstract and indexing annotation must be entered when the overall report is classified)

1 ORIGINATING ACTIVITY (Corporate author)
Naval Postgraduate School
Monterey, California 93940

2a. REPORT SECURITY CLASSIFICATION
Unclassified

2b. GROUP

3 REPORT TITLE
An Experimental Investigation of Asynchronous Demodulation of a Phase-Reversal Modulated Carrier

4 DESCRIPTIVE NOTES (Type of report and inclusive dates)
Technical Report - August, 1968

5 AUTHOR(S) (First name, middle initial, last name)
Francis A. Rudolph, Jr. — Commander, U. S. Navy
Glen A. Myers — Assoc. Prof., Naval Postgraduate School

6 REPORT DATE: August, 1968
7a. TOTAL NO. OF PAGES: 84
7b. NO. OF REFS: 14
8a. CONTRACT OR GRANT NO.
b. PROJECT NO.
c.
d.
9a. ORIGINATOR'S REPORT NUMBER(S): NPS-52MV8081A
9b. OTHER REPORT NO(S) (Any other numbers that may be assigned this report)

10. DISTRIBUTION STATEMENT
This document has been approved for public release and sale; its distribution is unlimited.

11. SUPPLEMENTARY NOTES

12. SPONSORING MILITARY ACTIVITY
Naval Ship Systems Command
Code 6050

13. ABSTRACT

This report considers an asynchronous (non-coherent) method of demodulating a carrier that is phase-reversal modulated by a two-level waveform. The comparatively simple demodulation technique treated relies on the conversion of a phase-modulated (PM) signal to an amplitude-modulated (AM) signal by appropriate filtering of the frequency components of the received phase-reversal modulated carrier. The resulting AM signal is then detected with a conventional envelope detector and the digital data is recovered with appropriate threshold and logic circuits.

The experimental asynchronous demodulation system requires approximately 12 db greater signal-to-noise power ratio for the same probability of error relative to the optimum performance of the coherent demodulation system. Thus with a signal-to-noise ratio of 18 db or greater, the asynchronous demodulation system has a measured probability of error of 10^{-3} or less; a signal-to-noise ratio of 23 db provides a measured probability of error of about 10^{-5}. Apart from simplicity, the asynchronous demodulation system has the advantage of not requiring prior knowledge of the transmitted signal's precise characteristics as is required in some coherent demodulation systems.

14 KEY WORDS	LINK A		LINK B		LINK
	ROLE	WT	ROLE	WT	ROLE
Phase Modulation					
Phase-reversal Modulation					
Biphase Modulation					
Phase-shift Keying					
Phase Detectors					
Asynchronous Phase Detectors					
Coherent Phase Detectors					
PM-to-AM Conversion					